

OPEN ACCESS

EDITED BY Xia Wang,

Chengdu University of Technology, China

REVIEWED BY Xiao Gao.

Shandong University of Science and

Technology, China

Zhixin Ma

Chengdu Geological Survey Center, China

*CORRESPONDENCE

Hengye Wei

My.wei@swpu.edu.cn

RECEIVED 28 July 2025
ACCEPTED 08 September 2025
PUBLISHED 30 September 2025

CITATION

Zou Y, Wei H, Mansour A, Wen Y and Fu X (2025) Carbonate platform demise across the Triassic-Jurassic transition in the Qiangtang Basin, Tibetan Plateau. *Front. Mar. Sci.* 12:1674649. doi: 10.3389/fmars.2025.1674649

COPYRIGHT

© 2025 Zou, Wei, Mansour, Wen and Fu. This is an open-access article distributed under the terms of the Creative Commons Attribution License (CC BY). The use, distribution or reproduction in other forums is permitted, provided the original author(s) and the copyright owner(s) are credited and that the original publication in this journal is cited, in accordance with accepted academic practice. No use, distribution or reproduction is permitted which does not comply with these terms.

Carbonate platform demise across the Triassic-Jurassic transition in the Qiangtang Basin, Tibetan Plateau

Yi Zou¹, Hengye Wei^{1*}, Ahmed Mansour^{1,2}, Yue Wen¹ and Xiugen Fu¹

¹School of Geoscience and Technology, Southwest Petroleum University, Chengdu, China, ²Geology Department. Faculty of Science. Minia University. Minia. Egypt

Introduction: Carbonate platforms are highly sensitive to environmental, climatic, and oceanographic changes. The demise of carbonate platform is often associated with perturbations in oceanic chemistry and/or sea level rise, which are also the modern environmental challenges for human being. However, the main causes behind the carbonate platform demise are still a matter of significant debate.

Methods: Here, we present nitrogen $(\delta^{15}N_{bulk})$ and carbon isotopes of bulk carbonate $(\delta^{13}C_{carb})$ and organic $(\delta^{13}C_{org})$ geochemistry data, mercury (Hg), pyritic framboids size distributions, and major element content, from the upper Sobucha Foramtion (Upper Triassic) to the lower Quse Formation (Lower Jurassic) in the Wenquan section of the Qiangtang Basin (Tibet) of the eastern Tethyan domain.

Results: The results show that the carbonate platform demise was preceded by a negative excursion of $\delta^{15}N_{bulk}$ and severe reducing, mainly euxinic conditions in shallow marine settings before the Triassic-Jurassic (T-J) boundary. This was followed by a negative excursion of carbon isotope data, coincident with an extremely positive shift in mercury composition at the T-J boundary.

Discussion: The nitrogen excursion suggests that eutrophication, likely resulting in partial assimilation of nitrogen, and euxinia in the euphotic zone may have depressed the ecosystem prior to the demise of carbonate platform. Conversely, δ^{13} C excursion and elevated Hg levels reveal that large-scale isotopically light carbon emissions probably controlled by widespread volcanism of the Central Atlantic Magmatic Province (CAMP) were the ultimate trigger of the carbonate platform demise.

KEYWORDS

carbonate platform, end-Triassic, nitrogen isotope, carbon isotope, redox conditions, Tibetan Plateau

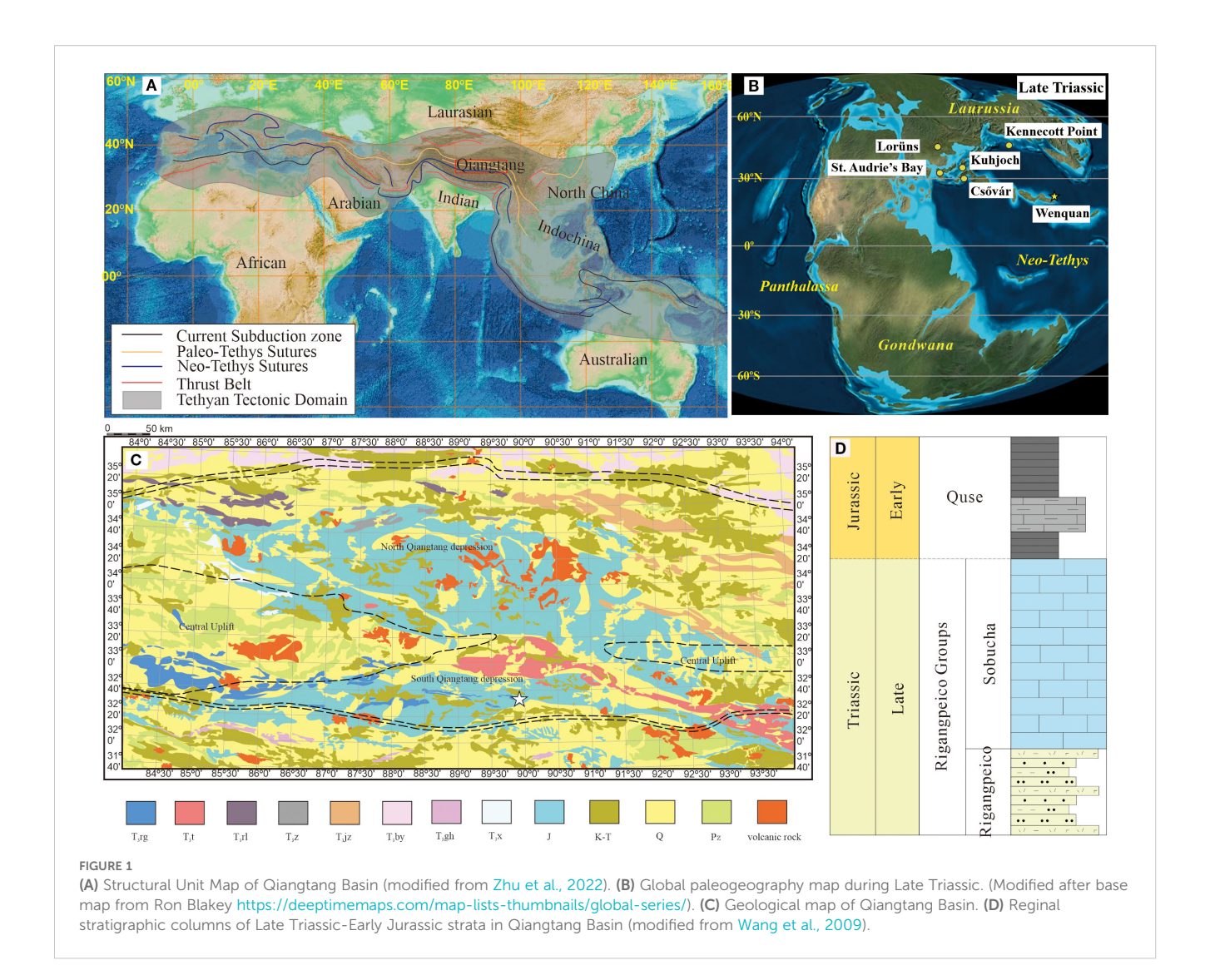
1 Introduction

The demise of ancient carbonate platforms has been induced by a complex interaction of environmental, biological, oceanographic, and eustatic sea level changes (Schlager, 1981; Bahamond et al., 1997; Marino and Santantonio, 2010; Paul et al., 2025). Across Earth's history, several carbonate platform demise events were reported, such as in the Northern Calcareous Alps (Gázdzicki et al., 1979), Steinplatte platform (Felber et al., 2015), platforms in Italy (Apennine carbonate platform, Trecalli et al., 2012; Mesozoic Adriatic carbonate platform, Brčić et al., 2021), the Dachstein platform in the Transdanubian Range (Pálfy et al., 2021), and the Queensland Plateau (Betzler et al., 2024). Although some resilient carbonate platforms can recover after the environmental crises (Maurer et al., 2008; Al-Suwaidi et al., 2016; Ge et al., 2018; Todaro et al., 2022; Urban et al., 2023; Montanaro et al., 2024), some transformed to be long-term deposits of siliciclastic sediments, particularly shales/mudstones (Zhang et al., 2024; Martínez-Rodríguez et al., 2025), indicating their permanent demise of the platforms. Several factors have been suggested to explain the demise of a carbonate platform, including rapid sea level rise (Schlager, 1981), environmental stressors such as severe anoxia, eutrophication conditions, extreme climate warming, and/or ocean acidification (Mutti and Hallock, 2003; Hallock and Schlager, 1986), increased siliciclastic influx (Wilson, 2008), and biological factors such as widespread extinction of key carbonate-producing biota (Flügel and Kiessling, 2002). Despite the relative significance of these factors, the ultimate reasons for the carbonate platform demise are still debated, particularly the role of eustatic sea-level changes and environmental stressors.

The T-J boundary is a crucial turning point in geological history, marked by massive volcanism linked to the CAMP, the early stages of the Atlantic Ocean rifting, and widespread biotic extinction (Hesselbo et al., 2002; Pálfy, 2003; Galli et al., 2005; Felber et al., 2015; Davies et al., 2017; Todaro et al., 2022; Rigo et al., 2024). The geological events could trigger a cascade of regional- to global-scale environmental changes, such as global warming, oceanic acidification, marine anoxia, eustatic sea level rise (Pálfy et al., 2001; Carter and Hori, 2005; Kiessling et al., 2007; Greene et al., 2012; McRoberts et al., 2012; Trecalli et al., 2012; McElwain et al., 1999; Fujisaki et al., 2020; Fox et al., 2022; Chen et al., 2023). Additionally, intensified continental weathering (Fujisaki et al., 2020; Shen et al., 2022) disrupted ocean chemistry and carbonate productivity (Hautmann et al., 2008; Van De Schootbrugge et al., 2008; Greene et al., 2012; McRoberts et al., 2012). These environmental disturbances would offer a valuable opportunity to study the causes for carbonate platform demise across the T-J boundary transition. For example, the oceanic anoxia and/or acidification have been suggested to be the main drivers behind the disappearance of the benthic faunas (foraminifera, corals) and the demise of carbonate platform in the upper Rhaetian of the classic Lombardy Basin section, Italy (Galli et al., 2005), and in the western Northern Calcareous Alps (NCA), Austria (McRoberts et al., 1997; Felber et al., 2015). These studies are focused on western Tethyan Ocean, while the eastern Tethyan region have received little attention. Located within the Eastern Tethyan Domain, Tibet represents the largest and most continuous marine stratigraphic region in China. The Qiangtang Basin, in particular, represents the largest plate with complete Mesozoic deposition in the Tibetan Plateau (Zhao et al., 2001; Wang et al., 2004, 2009, 2020). The southern part of the basin received a large set of carbonate sediments in the Late Triassic, which transformed into a thick interval of black shales in the Early Jurassic (Wang and Fu, 2018; Wang et al, 2020). This shift implies a key marker of the carbonate platform collapse during the T-J transition, offering a significant opportunity to investigate the debate of causes and mechanisms of this phenomenon. Here, we present a new dataset of nitrogen and carbon isotopes, mercury geochemistry, pyritic framboids size distributions, and major elements contents, from the Upper Triassic upper Sobucha Foramtion to the Lower Jurassic Quse Formation in the Wenquan section in the Qiangtang Basin. These data are conducted to address marine redox conditions, nitrogen cycling, carbon burial, and active volcanism during the T-J boundary transition and to assess their impact on the carbonate platform demise in this region.

2 Geological setting

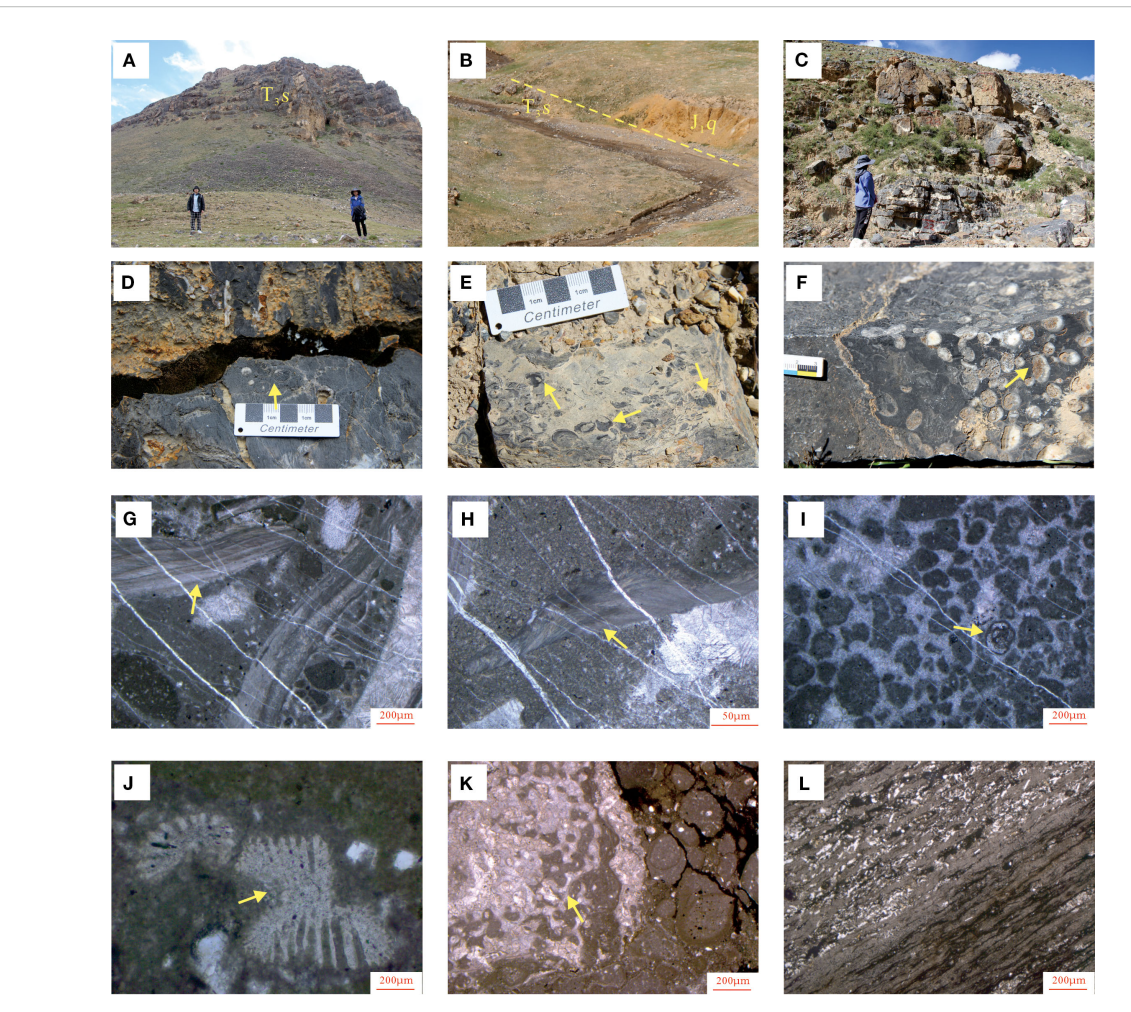
The Qiangtang Basin is one of the largest Mesozoic marine basins in China, formed on the pre-Ordovician basement of the Qiangtang Block in the hinterland of the Tibetan Plateau (Figure 1C). Tectonically, it occurs in the eastern segment of the Tethyan tectonic domain (Figure 1A, B) (Tan et al., 2002; Liu et al., 2007; Fu et al., 2016). The basin is bordered by two sutures, the Bangong-Nujiang suture (BNS) to the south and the Hoh Xil-Jinshajiang suture to the north, leading to its subdivision into the South Qiangtang depression, Central Uplift, and North Qiangtang depression (Wang et al., 2022). During the early Permian, the North Qiangtang Terrane was controlled by continuous northward drifting from the Gondwana supercontinent. By the Late Triassic, the North Qiangtang Terrane had collided with the southern margin of the Eurasian Plate along the Jinshajiang Suture Zone, marking the end of closure of the Paleo-Tethys Ocean (Figure 1B) (Song et al., 2017). This was followed by the amalgamation of North Qiangtang Terrane with the South Qiangtang Terrane, which had already positioned along the southern margin of Eurasia, via the Longmu Co-Shuanghu Suture Zone (Metcalfe, 2013; Song et al., 2012, 2017; Yan et al., 2018). Furthermore, rapid northward displacement of the Qiangtang Basin during the Triassic led to a strong collision with the Hoh Xil-Songpan Block and the development of complex systems of thrust-folds and syn-tectonic foreland structures (Fang et al., 2016). By the Early Jurassic, the Qiangtang Basin further drifted toward mid-paleolatitudes of the Meso-Tethys Ocean. This resulted in the development of lacustrine settings in the North Qiangtang Terrane, while pelagic-hemipelagic open ocean conditions were prevalent in the South Qiangtang Terrane (Wang et al., 2022). During the Early Cretaceous, the Indian Plate separated from Gondwana and progressively drifted northward, resulting in the gradual narrowing toward the eventual



closure of the Neo-Tethys Ocean (Sengör, 1979; Stampfli and Borel, 2002; Angiolini et al., 2003). This further controlled the collision between the Lhasa and Qiangtang blocks and the formation ofthrust fold belts in the BNS (Zhu et al., 2022).

The Qiangtang Basin underwent a complete cycle of sedimentary filling with marine deposits during the opening of Neo-Tethys Ocean (Figure 1B) (Wang et al., 2009). The exposed Mesozoic strata in the southern Qiangtang Basin mainly include the Upper Triassic Riganpeico groups (T₃rg), which is represented by the Riganpeico and Sobucha Formations (Wang and Zheng, 2007). The Upper Triassic Sobucha Formation (T₃s) is predominantly composed of a thick interval of mudstones, siltstones, and sandstones. The Lower Jurassic Quse Formation (J₁q) consists of mudstones with argillaceous lumps, shales, and bioclastic limestones and packstones, intercalated with limestone. The Middle Jurassic Sawa Formation (J₂s) is dominated by mudstones and shales (Figure 2D). The studied Wenquan section (89° 56′ 23″ E, 32° 21′ 48″ N) is located in a valley beside the Wenquan hot springs at Sewa in the town of Shuanghu area in the Qiangtang

Basin. The Wenquan section is represented by a thick stratigraphic succession of the Sobucha (T_3s) and Quse (J_1q) Formations (Figure 2). Field observations of the study section reveal a distinct lithological contact between the limestone of the Sobucha Formation and the shale of the Quse Formation (Figures 2A, B), potentially marking the T-J boundary. The field observations of the Sobucha Formation exhibit thin- to medium-bedded limestones, pack- to wackestone, and medium- to thick-bedded grainstones, with occasional nodular limestones (Figure 2C), and calcareous mudstones. The bioclasts are dominated by gastropods (Figure 2D), bivalves (Figure 2E), corals (Figure 2F), brachiopods (Figures 2G, H), foraminifera (Figure 2I), echinoderms (Figure 2J), and sponges (Figure 2K). The high diversity of fauna represents open shallow carbonate platform facies. The total thickness of the Sobucha Formation limestones is more than 100 m. In contrast, the Quse Formation yielded scarce fossil debris and is dominated by thinbedded calcareous mudstones and shales with laminations (Figure 2L), indicating deeper shelf environments. The total thickness of the Quse Formation shale is more than 500 m.



Field and thin section observation of the Wenquan section. (A) Limestones of the Sobucha Formation. (B) The Sobucha—Quse formation boundary. (C) Nodular limestones. (D) Gastropods in grainstone. (E) Bivalves in grainstone. (F) Colonial coral. (G, H) Brachiopods in packstone, sample WQ-34 (I) Foraminifera in grainstone, sample WQ-21. (J) Echinoderms in mudstones, sample WQ-27. (K) Sponges in grainstone, sample WQ-78. (L) Shales with lamination, sample WQ-104.

3 Methods

A total of 108 rock samples of limestones and shales were collected for thin section observations and geochemical analyses. Sampling was conducted on fresh, unweathered outcrop surfaces with uniform lithology and avoiding veins. Total organic carbon (TOC) content and bulk-rock elemental analyses were measured at the School of Geoscience and Technology, Southwest Petroleum University. Approximately 100 mg of each powdered sample was subjected to acid digestion using diluted HCl acid within permeable ceramic crucibles to remove inorganic carbon minerals. The residual organic matter was rinsed repeatedly with deionized water until neutral pH is reached. The residue was dried and analyzed using a high-frequency infrared carbon-sulfur analyzer (model: TL851-6K). For analytical control, one replicate sample and a standard were analyzed per twelve samples. Analytical precision was better than 0.5 wt%. Major oxides were determined using an energy-dispersive X-ray fluorescence (XRF) spectrometer via pressed powder pellets.

Carbonate carbon and oxygen isotopic compositions were measured using a Delta-Q isotopic ratio mass spectrometer (IRMS) at the Southwest Petroleum University. One replicate sample and a standard were analyzed per ten samples. Bulk powder samples of 0.2 to 1 mg were flushed by helium gas in a vial for 580 seconds and then reacted with pure phosphoric acid at 70°C for 1 hour. The evolved gas (CO₂) from the headspace of the vials was analyzed using a Thermo Fisher Scientific (Bremen) GasBench Plus connected to the Delta-Q IRMS. All data are reported as per mil variation (‰) relative to Vienna Pee Dee Belemnite (VPDB). The analytical precision of $\delta^{13}C$ and $\delta^{18}O$ measurements was better than 0.08‰ based on replicate analyses of the lab standard GBW04416.

For $\delta^{15}N_{bulk}$ measurements, powdered samples were treated with diluted HCl acid to remove inorganic carbon, followed by treatment with HF acid to eliminate silicate minerals. The residue is rinsed to neutrality, dried, and ground to a particle size of <75 μ m (passing a 200-mesh sieve). Between 0.2 and 5 mg of the residual sample powder was weighed in a tin capsule and compactly

wrapped into a cube. The capsule is then automatically introduced via an elemental analyzer (EA) autosampler into a hightemperature oxidation reactor (980°C) under a helium carrier gas stream. Within this oxygen-enriched environment, the sample undergoes flash combustion, instantaneously oxidizing to produce a gaseous mixture including NO, N2O, N2O2, N2, CO, CO2, H2O, and SO2. This gas stream subsequently passes through a reactor containing chromium oxide and silvered cobaltous oxide, where CO is oxidized to CO2, and SO2 and halogen gases are removed. The gases then enter a reduction reactor (650°C) packed with copper wire, where the nitrogen oxides are reduced to N2, and any excess oxygen is absorbed. The resulting gases flow through a chemical trap for H₂O removal and CO₂ absorption. N₂ is then separated from any residual gases using a gas chromatographic column and is directed to a thermal conductivity detector for quantification of total nitrogen content. Concurrently, a small, continuous stream of the separated N2 gas is routed via a ConFlo IV interface to an isotope ratio mass spectrometer (Delta Q IRMS) coupled online with the EA for measurement of nitrogen isotope ratios (δ^{15} N). Replicate measurements of standard USGS40 yield an analytical precision (1 σ) better than 0.15% for $\delta^{15}N$ values, which are reported relative to atmospheric nitrogen.

For pyrite morphology observations and pyritic framboid size measurements were conducted via a Laser-Induced Break down Spectroscopy (LIBS) at Southwest Petroleum University. Framboidal pyrite morphology and size measurements were performed exclusively on samples with geochemical isotopic excursions around the T-J boundary. Both normal and infilled framboids were included in the statistical analysis.

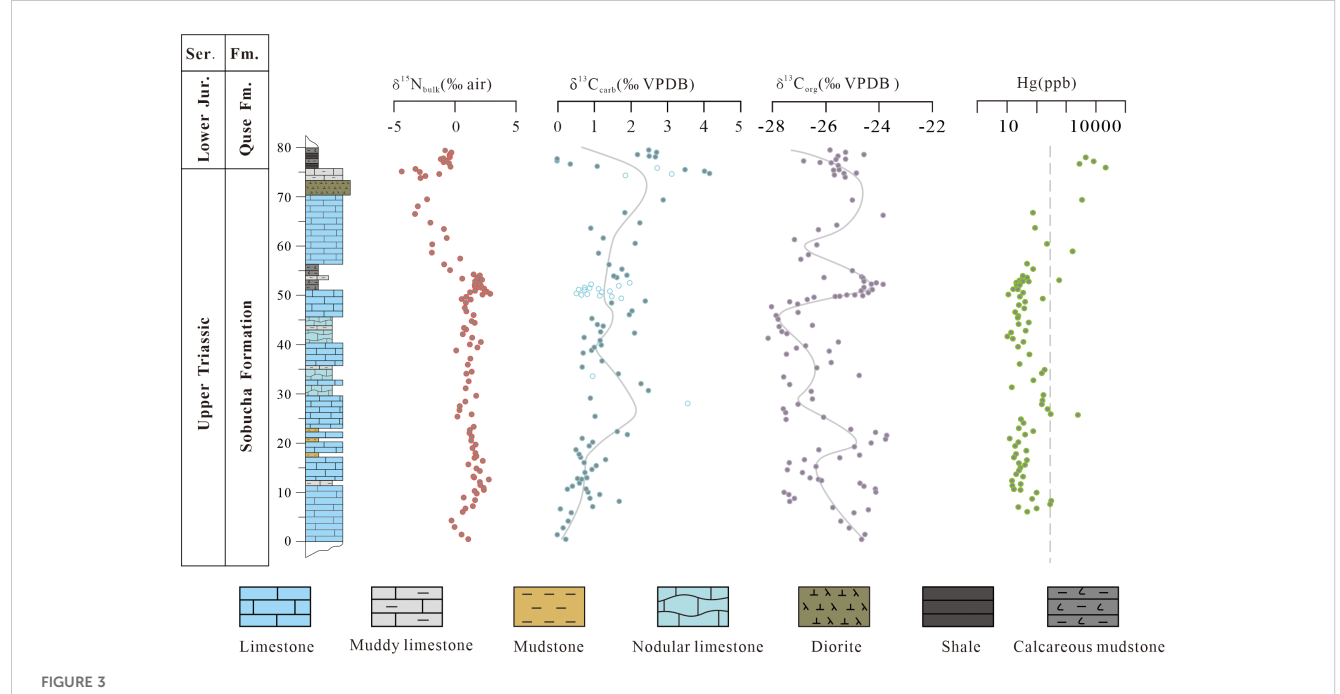
Hg concentrations were analyzed using a Direct Mercury Analyzer (DMA80) at the China University of Geosciences (Wuhan). Results of low-Hg and high-Hg samples were calibrated to the standards GBW07424 (33 \pm 4 ppb Hg) and GBW07403 (590 \pm 80 ppb Hg), respectively. One replicate sample and a standard measurement were analyzed per ten unknown samples. Data quality was monitored via multiple analyses of the standards GBW07424 and GBW07403, yielding an analytical precision (2 σ) of \pm 0.5% of the reported Hg concentrations.

4 Results

4.1 Carbon and nitrogen isotopic compositions

The bulk carbonate carbon isotope composition ($\delta^{13}C_{carb}$) of the Wenquan section exhibits a range of -1.4 % to 4.9% (mean = 1.2%). In the lower Sobucha Formation, the $\delta^{13}C_{carb}$ profile shows the first positive excursion from 1.2% to 4.9%, with a magnitude of about 3.7%. A secondary positive excursion occurs in the upper part of the formation, ranging from 0.9% to 3.7%, with a magnitude of about 2.6%. Notably, a pronounced negative excursion is observed close to the T-J boundary, where values decline sharply from 4.02% to 0.02% (4% on magnitude) (Figure 3).

Organic carbon isotope ($\delta^{13}C_{\rm org}$) values of the Wenquan section range from -29.15 ‰ to -23.71‰ (mean = -25.97‰). The lower Sobucha Formation records a positive excursion from -27.39‰ to -23.71‰, with a magnitude of about 3.68‰, exhibiting a significant



Chemostratigraphic composition various isotopic and elemental proxy data, including from left to right, the $\delta^{15}N_{\text{bulk}}$, $\delta^{13}C_{\text{carb}}$, $\delta^{13}C_{\text{carb}}$, and Hg at the Wenquan section. $\delta^{13}C_{\text{carb}}$ and $\delta^{13}C_{\text{carb}}$ curves were smoothed using LOESS. Samples with Mn/Sr ratios greater than 2 are represented by open symbols on the $\delta^{13}C_{\text{carb}}$ curve.

chemostratigraphic lead relative to the coeval $\delta^{13}C_{carb}$ excursion. The middle part shows the second positive excursion from about -27.49‰ to -25.79 ‰, with a magnitude of about 1.7‰. The uppermost stratigraphic interval exhibits a negative trend synchronous with the $\delta^{13}C_{carb}$ excursion, decreasing from -24.86‰ to -27.20‰, with a magnitude of about -2.34‰.

The $\delta^{15}N_{bulk}$ curve shows values ranging from -4.32% to 3.03% (mean = -0.76%). A prominent negative $\delta^{15}N_{bulk}$ excursion is recorded in the uppermost Sobucha Formation, close to the T-J boundary, with values decreasing from -0.31% to -4.32%, showing a magnitude of 4.01%. Values return to background levels within the Quse Formation (Figure 3). The negative $\delta^{15}N_{bulk}$ excursion coincides with the positive excursions in $\delta^{13}C_{carb}$ and $\delta^{13}C_{org}$ profile. This interval is also characterized by a concurrent increase in phosphorus (P) content. Other geochemical proxies fail to demonstrate statistically significant covariation patterns across the studied succession (Figure 4).

4.2 Pyrite morphologies

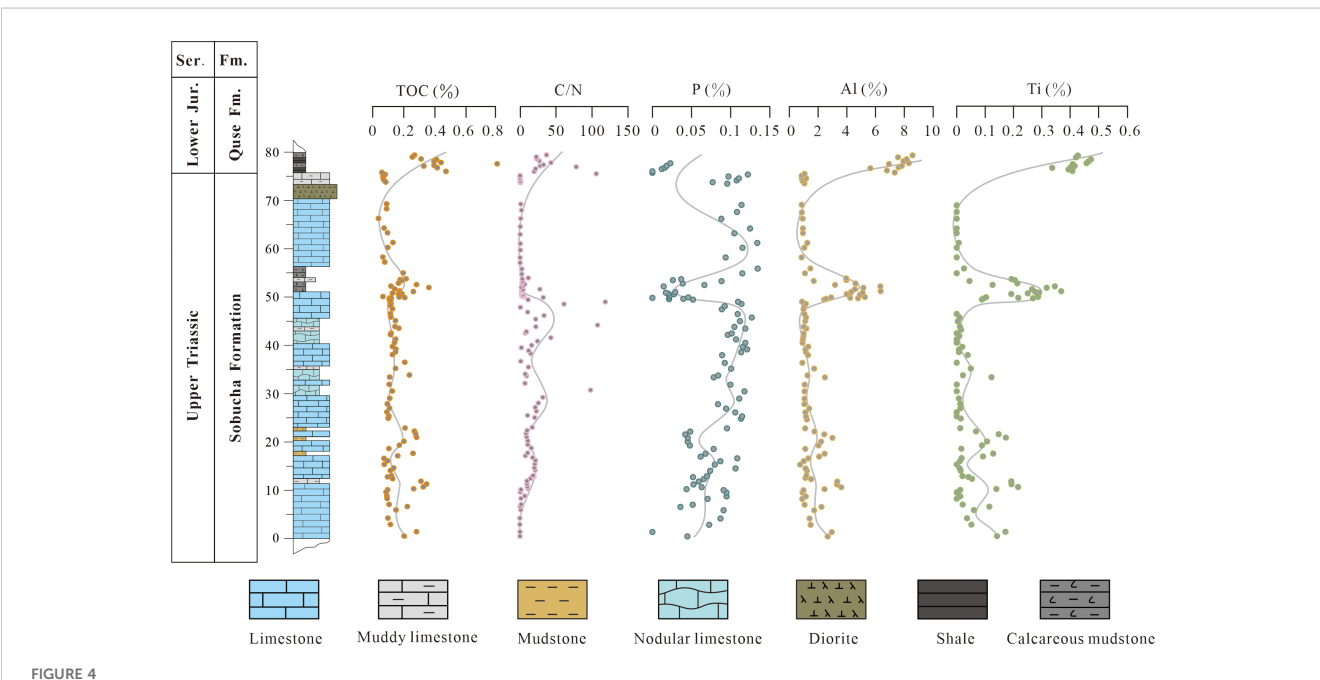
In this study, framboidal pyrite exhibits a mean diameter ranging from 4.59 μm to 11.52 μm. The minimum framboid diameter ranges from 2.21 μm to 7.04 μm, while the maximum framboid diameter ranges from 9.21 μm to 64.39 μm. The standard deviation of the measured diameters is in the range of 1.26-to 6.97 μm. Variable pyrite morphologies are observed, including normal framboids (Figures 5A, B), overgrown framboids (Figure 5C), euhedral pyrites (Figure 5D), and infilled framboids (Figures 5E, F). Infilled framboids are round and show indistinct small holes, suggesting a framboidal origin (Figure 5E). With progressive

infilling, the infilled framboids may become pyritic masses which show round or irregular form lacking any texture inside (Figure 5D). Overgrown framboids show large euhedral pyrites in the outmost of previously formed framboids (Figure 5E). In summary, infilled framboids, pyrite masses, and overgrown framboids represent intermediate forms of pyrite, indicating the transformation of framboids (Sawlowicz, 1993). The diameters of normal or infilled framboids are measured for the size distributions.

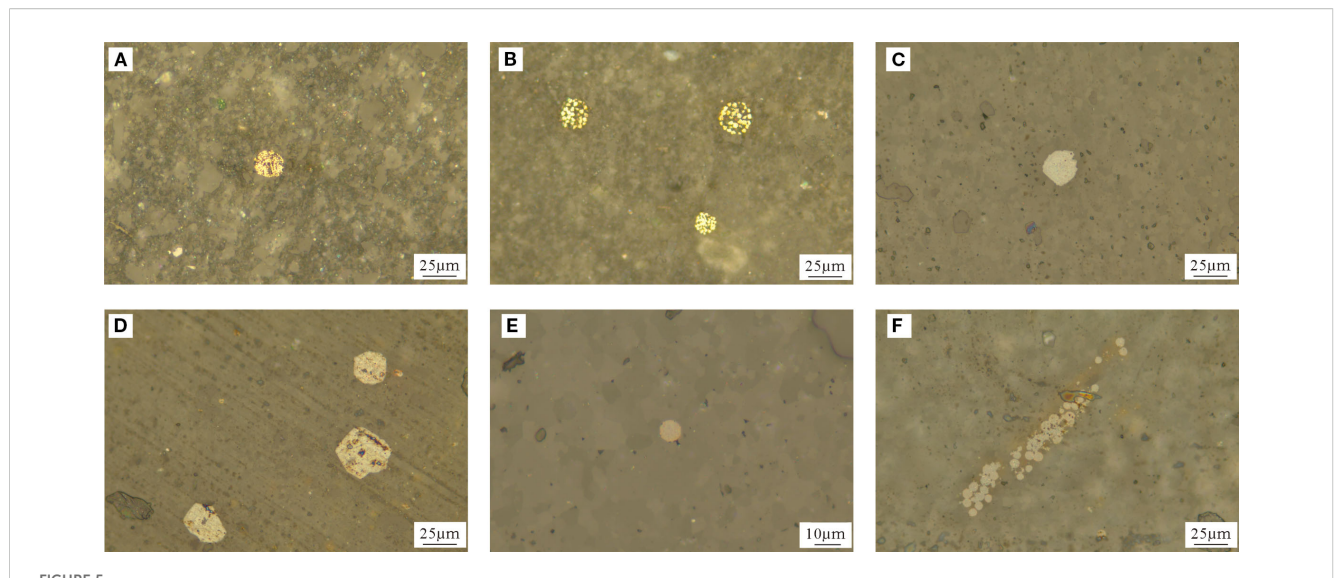
4.3 TOC and mercury contents

Throughout the Wenquan section, TOC content varies from 0.07-0.84 wt.% (averaging 0.18 wt.%). The Sobucha Formation shows significantly low TOC values, with an average of 0.15 wt.%, contrasting sharply with the overlying Quse Formation which shows slightly higher organic carbon abundance (mean = 0.50 wt.%, max = 0.84 wt.%; Figure 4).

The Hg content exhibits variable concentrations with values are in the range of 10 ppb to 21930 ppb (mean = 580 ppb). The Hg content shows a slight increase (~2500 ppb) at the upper Sobucha Formation, reaching to the highest Hg concentrations in the lowermost Quse Formation (lowermost Jurassic) (Figure 3). Organic matter is widely recognized as the dominant Hg host phase in reducing sediments (Mazrui et al., 2016). However, there is no correlation between Hg and TOC, and other elements, such as S, Al, and K (Figure 6), probably owing to the lower values of TOC, sulfur, or clay content. Therefore, the Hg concentrations represent the true Hg variation without TOC normalization (Font et al., 2021). Therefore, the pronounced enrichment of Hg anomaly at the T-J boundary (20,000 ppb) represent high Hg input to the ocean (Figure 3).



Chemostratigraphic composition various elemental proxy data, including from left to right, the TOC, C/N, P, Al, and Ti at the Wenquan section, all the curves were smoothed using LOESS.



Pyrite morphologies under reflected light. (A, B) Normal framboids showing uniform microcrystals, sample WQ-77. (C) Overgrown framboids showing regular idiomorphic outlines, sample WQ-96. (D) Euhedral pyrite, sample WQ-78. (E) Infilled framboid, sample WQ-95. (F) Clustered framboids, sample WQ-91.

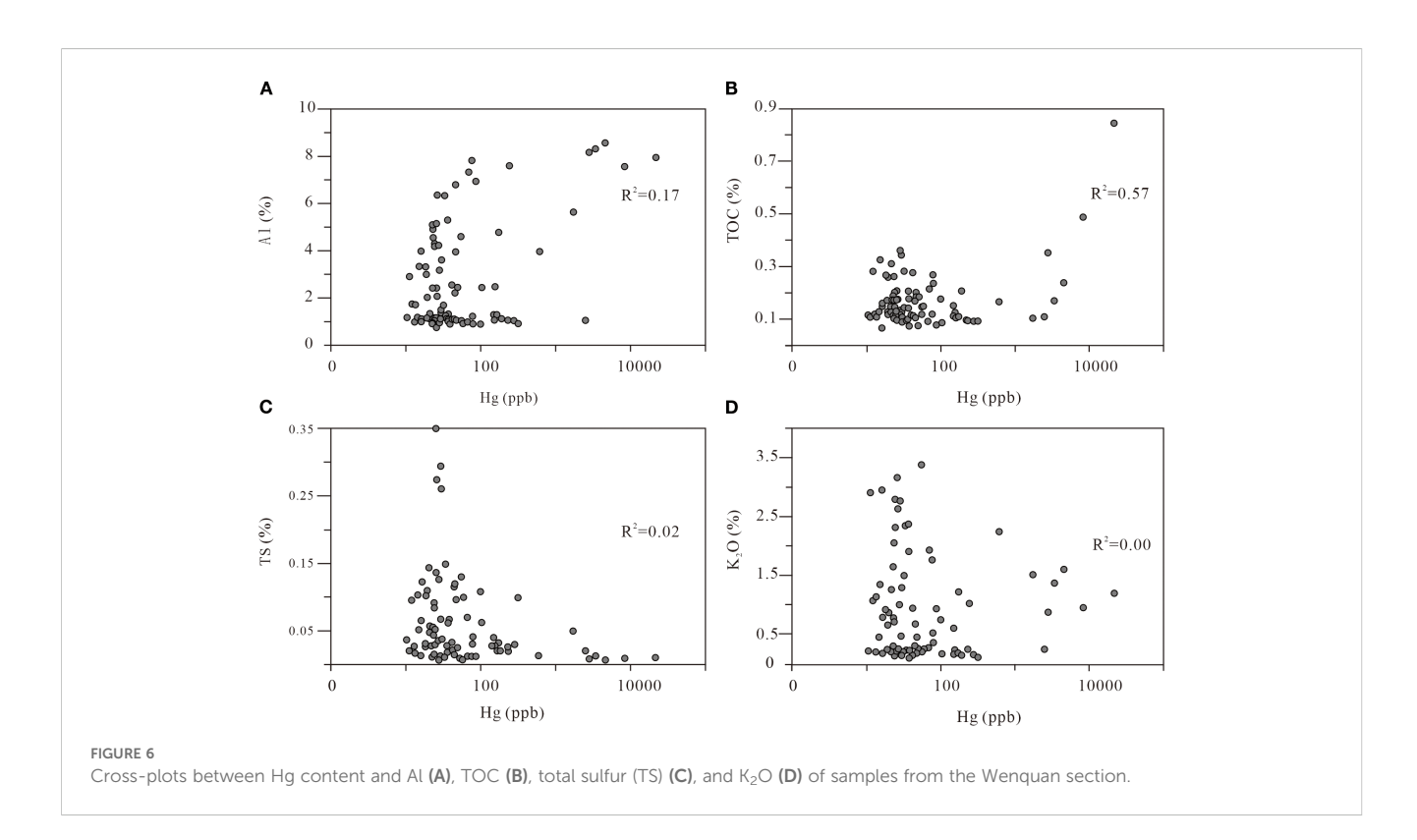
5 Discussion

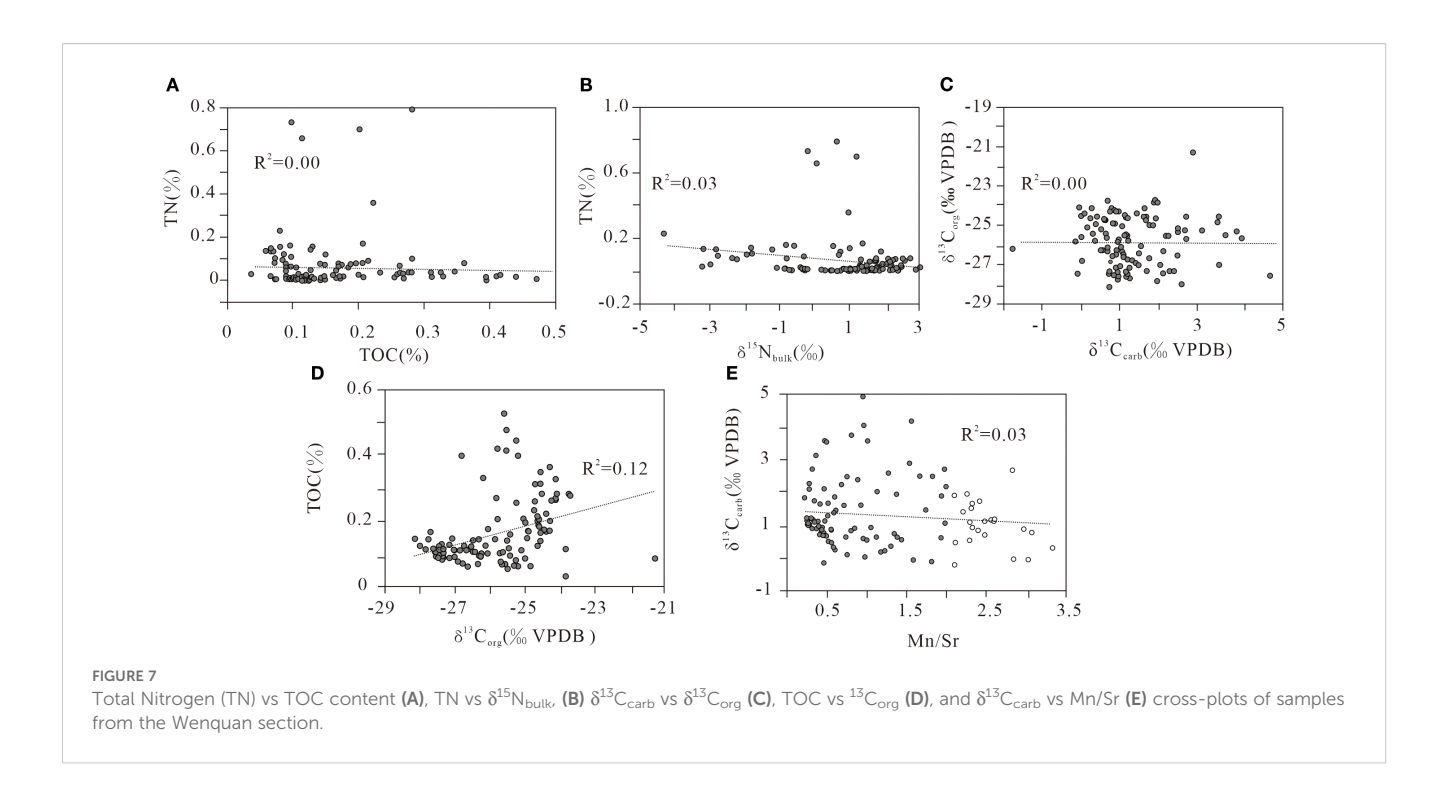
5.1 Assessing the primary signal of the carbon and nitrogen isotope ratios

Sedimentary $\delta^{13}C$ and $\delta^{15}N$ isotope records serve as reliable proxies for reconstructing oceanic biogeochemical cycling and elemental fluxes during geological intervals. However, signatures are

susceptible to diagenetic alteration, necessitating rigorous assessment of primary geochemical preservation (Veizer et al., 1999; Kuypers et al., 2004; Junium and Arthur, 2007; Saltzman et al., 2012; Higgins et al., 2012; Liu et al., 2016; Ruvalcaba Baroni et al., 2015; Zhang et al., 2019). A series of cross plots are provided (Figure 7) to evaluate the potential influence of diagenesis on the isotope records.

The absence of covariation between TN and TOC (Figure 7A) may indicate distinct sources for these components or the





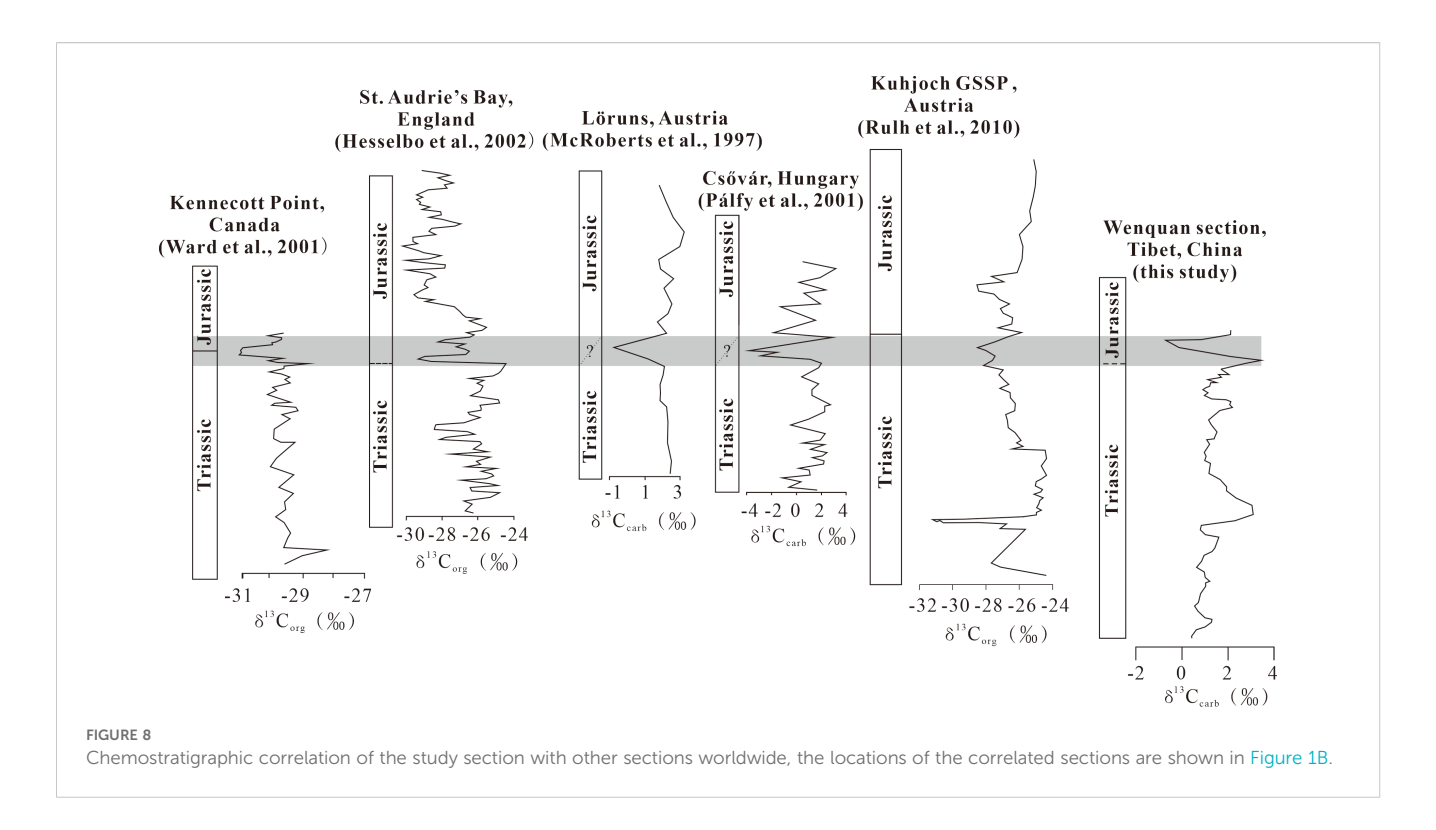
incorporation of nitrogen released from organic matter into K-rich clay minerals. This is consistent with the lack of significant correlation between the $\delta^{15}N$ composition and TN content (Figure 7B), contrasting with the expected negative trend from preferential decomposition of 14N-enriched compounds during diagenesis, suggesting primary nitrogen isotopic signals (Freudenthal et al., 2001; Lehmann et al., 2002). Organic carbon isotopes show stronger regional terrigenous influences, as evidenced by the poor correlation between $\delta^{13}C_{carb}$ and $\delta^{13}C_{org}$ data (Figure 7C). The poor correlations between the $\delta^{13}C_{org}$ values with TOC content support an insignificant influence of thermal degradation of organic matter and, therefore, near-primary $\delta^{13}C_{org}$ signatures (Figure 7D) (Luan et al., 2024). The Mn/Sr ratios are predominantly less than 2, with a minority of samples exceeding this threshold, which are not considered during the interpretation. All these suggest a limited influence of diagenesis on $\delta^{13}C_{carb}$ value (Figure 7E) (Kaufman et al., 1997; Derry et al., 1994; Korte et al., 2006). In other words, the bulk nitrogen and carbon isotope data analyzed in the Wenquan section preserve the original isotopic signatures. Although some organic carbon isotope values exhibit regional terrigenous influence, the synchronous variations in $\delta^{13}C_{org}$ and $\delta^{13}C_{carb}$ near the T-J boundary intervals likely reflect global-scale environmental changes (Figure 3) (Knoll et al., 1986; Oehlert and Swart, 2014).

5.2 Carbon cycle disturbance and global correlation

The preferential uptake of ¹²C during photosynthesis imparts a significant carbon isotope fractionation in organic matter (Park and Epstein, 1960). Consequently, marine phytoplankton typically

exhibits $\delta^{13}C$ values that are substantially depleted in ^{13}C relative to the isotopic composition of dissolved inorganic carbon in the ocean-atmosphere system. From the perspective of $\delta^{13}C$ fractionation mechanism, perturbations in the $^{13}C/^{12}C$ ratio (i.e. carbon isotope excursions, CIEs) are frequently associated with environmental perturbations, which disrupt the established dynamic balance of carbon isotopes between the biosphere, hydrosphere, and atmosphere, leading to notable $\delta^{13}C$ excursions across various carbon reservoirs (Dickens et al., 1995; Hesselbo et al., 2000; Beerling and Berner, 2002).

A well-established high-resolution δ^{13} C curve spanning the T-J boundary was documented in the Lorüns section of the Austrian NCA (McRoberts et al., 1997), which shows a distinct negative CIE with a magnitude of ~3% within the transitional Schattwald Beds. Notably, the studied Wenquan section shows a negative CIE in both $\delta^{13}C_{org}$ and $\delta^{13}C_{carb}$ curves, with estimated magnitudes of 2.34% and 4‰, respectively (Figure 3), indicating consistent chemostratigraphic correlations among regional sections (Figure 8). Additionally, the severe negative excursion in the Wenquan section suggests a significant perturbation in the global carbon cycle that coincided with the end-Triassic biotic crisis. In the Austrian NCA, the onset of the negative CIE toward the T-J boundary is interpreted as reflecting a collapse in carbonate productivity (Felber et al., 2015). In Hungary, the clear records of a significant negative CIE (~3.5‰) at the T-J boundary in the Csővár section were attributed to a demise of the carbonate factory (Pálfy et al., 2001). Global correlation of δ^{13} C records across the T-J boundary (Figure 8) suggest different magnitudes of excursion in carbon isotope profiles, with ~2% in Canada (Ward et al., 2001), ~4‰ in England (Hesselbo et al., 2002), ~3‰ in Austria (McRoberts et al., 1997; Ruhl et al., 2010), ~6‰ in Hungary (Pálfy et al., 2001), and ~4‰ in this study. The heterogeneity in



magnitudes of the CIE likely reflects varying degrees of diagenetic overprinting and/or local environmental factors superimposed on the global signal. Additionally, the negative CIEs reveal a global chemostratigraphic phenomenon that is consistent with environmental instabilities and disruption of the global carbon cycle at the T-J boundary due mainly to the injection of a large amount of light carbon derived from volcanic sources rich in CO₂ or seafloor methane release (Hesselbo et al., 2002).

Hg concentrations in the sedimentary records are increasingly utilized as a proxy for tracking paleovolcanic activity due to the significant release of Hg during volcanic eruptions (Schuster et al., 2002; Pyle and Mather, 2003; Guevara et al., 2010). Hg occurs in marine sediments in various forms (Ravichandran, 2004; Selin, 2009), potentially generating sedimentary Hg enrichments when depositional fluxes exceed the sequestration capacity of organic particles (Grasby et al., 2019). A distinct, extremely high Hg level is observed in the Wenquan section, precisely coincides with the negative CIEs in both $\delta^{13}C_{carb}$ and $\delta^{13}C_{org}$ at the T-J boundary (Figure 3), which reflect a global environmental disturbance signal (Amanda and Peter, 2014). This suggests that large-scale volcanism may have contributed to the light carbon input into the ocean-atmosphere ecosystem, causing a global disruption in the carbon cycle. The most likely source of active volcanism in this period was the CAMP (Bachan et al., 2016; Zaffani et al., 2018; Heimdal et al., 2020; Ruhl and Kürschner, 2011, 2020; Lindstrom et al., 2021; Shen et al., 2022). The widespread volcanic clastic deposition in the Eerlongba Formation in lower Jurassic (Chen and Wang, 2009; Zeng et al., 2019) also supports this inference. However, the significant magnitude of the negative CIE, which exceeds >3%, points to that gas emissions from active volcanism along may not fully trigger the observed perturbations at the T-J boundary (Berner, 2003). Davies et al. (2017) proposed a paradigm shift, whereby the primary trigger for Late Triassic environmental perturbations was not the surface lava flows of the CAMP, but rather earlier, deep-seated intrusive magmatism. They argued that the thermal metamorphism and degassing of organic-rich sediments associated with these intrusions released vast quantities of greenhouse gases for the Kakoulima layered mafic intrusion in Guinea, probably have contributed to the release of significant volumes of greenhouse gases and thereby significantly perturbating the carbon cycle at this time.

5.3 Origin of $\delta^{15}N$ negative excursion and changes in marine redox structure

At the Wenquan section, a significant negative $\delta^{15}N_{bulk}$ excursion (~4.87‰) occurs at the end of the Triassic. Nitrogen represents a critical bio-limiting nutrient for marine phytoplankton and plays a crucial role in environmental, oceanographic redox conditions, and biogeochemical processes (Falkowski, 1997; Tyrrell, 1999; Ruvalcaba Baroni et al., 2015; Stüeken et al., 2016, 2021; Zhang et al., 2020). Negative δ¹⁵N_{bulk} excursions can arise from several processes, such as (1) partial nitrate assimilation, (2) dominance of nitrogen fixation, (3) anaerobic ammonium oxidation (anammox), or (4) direct assimilation of NH_{4+} by marine biota (Sigman et al., 2009; Sach and Repeta, 1999; Pantoja et al., 2002; Kuypers et al., 2004; Stüeken et al., 2016; Schoepfer et al., 2016). Given that marine nitrogen fixation typically yields minimum $\delta^{15}N$ values of ~ -1.3% (Higgins et al., 2012), the observed negative $\delta^{15}N_{\text{bulk}}$ excursion magnitude at Wenquan cannot be promoted solely by nitrogen fixation. Alternatively, the assimilation of isotopically light, reduced nitrogen species, such as NH₄₊, may have contributed to these low values (Higgins et al., 2012; Zhang et al., 2019). It was suggested that contemporaneous hydrothermal activity would

have introduced substantial nutrients into the marine ecosystem (Li et al., 2024; Du et al., 2024; Zhang et al., 2024). This may have stimulated the biological primary productivity, promoting both nitrogen fixation and direct assimilation of 15 N-depleted NH₄₊ from hydrothermal fluids, collectively driving the observed negative δ^{15} N_{bulk} excursion. Further evidence for an exogenous nitrogen source (potentially NH₄₊) of isotopically low values comes from anomalously low sedimentary C/N ratios (Figure 4) (Krishnamurthy and Bhattacharya, 1986).

Global perturbations in the nitrogen cycle occurred during the T-J boundary transition. At the Austrian Kuhjoch global stratotype section and point (GSSP), a pronounced positive $\delta^{15}N$ excursion with a magnitude of 3% at the end-Triassic coincident with a peak in TOC content, suggesting enhanced nitrate availability (Li et al., 2025). At Katsuvama section (Japan), two negative δ^{15} N excursions were recorded at the T-J boundary and in the Hettangian Stage (Fujisaki et al., 2020). Both negative excursion events are attributed to partial nitrate assimilation, indicating a nitrate-rich ocean setting at that time. In the Kennecott Point section (Canada), a significant negative δ¹⁵N excursion, reaching a magnitude of up to ~5‰, coincided with euxinic conditions, suggesting nitrogen cycle dominated by cyanobacterial nitrogen fixation and/or phytoplankton assimilation of 15N-depleted NH4+ from upwelled waters (Kasprak et al., 2015). Conversely, a positive δ^{15} N excursion associated with anoxic water masses was reported across the T-J boundary from the Mingolsheim core in Germany (Quan et al., 2008). Thus, the global heterogeneous records of $\delta^{15}N$ excursions during the T-J transition may reflect spatiotemporal variability in marine nitrogen cycling (Li et al., 2025).

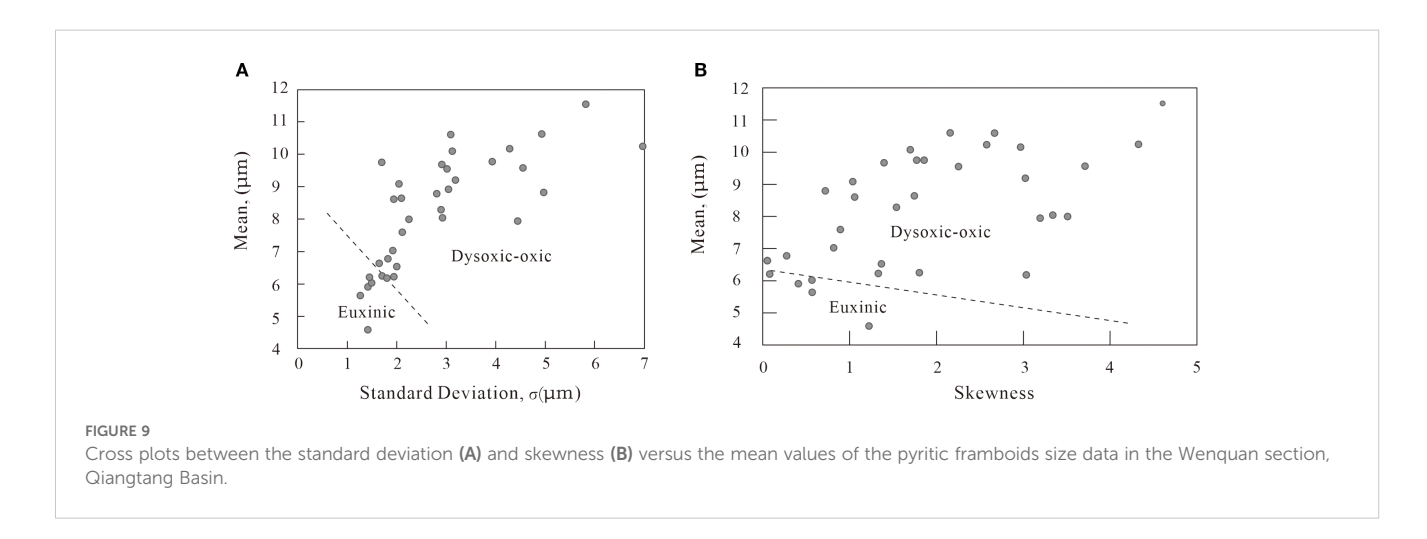
Here, marine redox conditions were assessed based on the framboidal pyrite size distribution and microscopic examination (Figures 9, 10). Under severe reducing conditions, such as anoxic-euxinic environments, framboids with smaller mean diameters (typically $< 5-6~\mu m$) and narrow size distributions are predominated, whereas oxic-dysoxic settings yield larger and more variable framboids (Raiswell, 1982; Wilkin et al., 1996). Cross-plots of framboid standard deviation versus mean diameter from Wenquan reveal that samples were deposited under fluctuating redox regimes, from euxinic to dysoxic-oxic

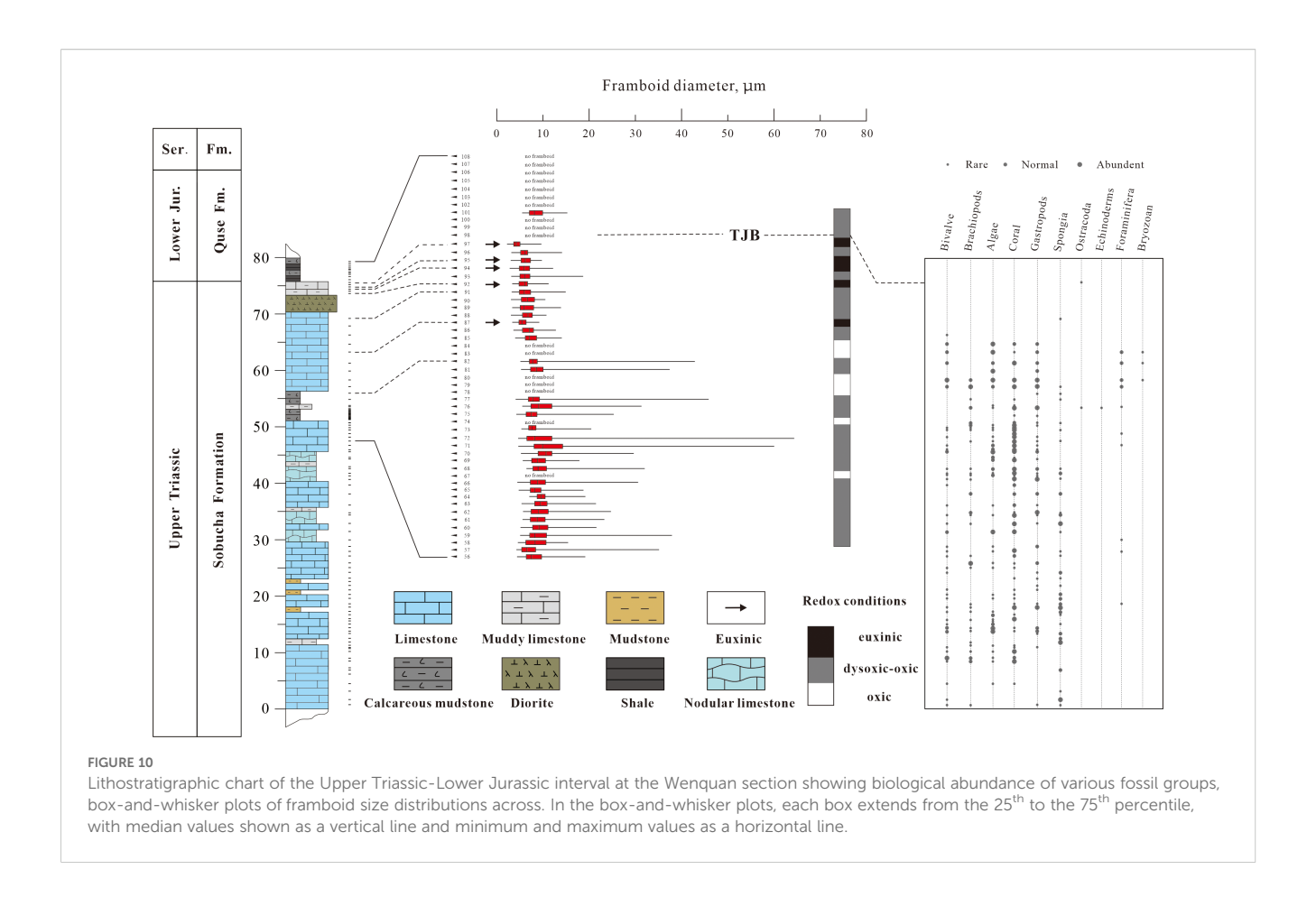
conditions (Figure 9). Additionally, the box-and-whisker plots of the framboid size distribution (Figure 10) suggest predominantly dysoxic-oxic conditions in the Upper Triassic, with a brief interval of euxinic conditions in the uppermost limestone interval at the end of the Triassic and prior to the T-J boundary. Although pyrite was not observed in some samples, well-developed horizontal lamination (Figure 2l) in the Quse Formation shale indicates dysoxic conditions to some extent (Tyson and Pearson, 1991). However, the euxinic conditions at the uppermost Triassic are not coincided with the negative $\delta^{15}N_{bulk}$ excursion, reinforcing the proposed interpretation of the assimilation origin of reduced nitrogen instead of denitrification as the primary mechanism.

5.4 Implication for carbonate platform demise

Carbonate platform demise is a complex process occurs in response to environmental and oceanographic instabilities, which can be triggered by multiple interacting factors. This includes rapid sea level rise (Schlager, 1981), tectonic subsidence (Bahamond et al., 1997; Föllmi and Gainon, 2008; Marino and Santantonio, 2010; Leonide et al., 2012; Pálfy et al., 2021; Martínez-Rodríguez et al., 2025), or environmental stressors such as ocean acidification, eutrophication, and marine anoxia (Philip and Airaud-Crumière, 1991; Trecalli et al., 2012; Fyhn et al., 2013; Felber et al., 2015; Todaro et al., 2017, 2022). Additionally, enhanced siliciclastic flux and climatic shifts can also contribute to the destabilization and demise of carbonate platforms via an increase in turbidity and light penetration, thereby limiting benthic carbonate-producing organisms (Hou et al., 2017; Jiang et al., 2019; Wu et al., 2022; Paul et al., 2025).

At Wenquan, the negative excursion in nitrogen isotope data precedes the carbonate platform demise, suggesting that eutrophication, possibly controlled by upwelling of nutrient-rich waters supplied sufficient isotopically light N for assimilation, was one of the main causes. Fujisaki et al. (2020) identified the vertical expansion of the mid-Panthalassic OMZ during the T-J boundary, which may be related to upwelling. This is supported by the





increasing P contents in this study section, which indicate intense upwelling (Kametaka et al., 2005). Euxinic conditions also occurred in the upper limestone succession before the carbonate platform demise, coincident with the disappearance of benthic fauna as evidenced by the decline in bioclast abundance distribution. This indicates that depressed ecosystem caused by anoxic-sulfidic conditions in shallow water settings may have played a significant role in suppressing the carbonate platform and destabilizing benthic biota, leading to the platform demise. Furthermore, the ultimate demise of the carbonate platform was associated with a major carbon cycle perturbation aligns with the onset of large-scale volcanism, suggesting massive volcanic outgassing most likely controlled by the CAMP. This indicates that the CAMP supervolcanism may be the ultimate fatal to the demise of the carbonate factory ecosystem via triggering cascade environmental changes such as global warming and/or acidification.

6 Conclusions

Here, new data of carbon (bulk carbonate and organic) and nitrogen isotope geochemistry, major elements, framboidal pyrite morphology, and Hg content were conducted across the T-J boundary at the Wenquan section in the Qiangtang Basin. Synchronous negative CIEs in both $\delta^{13}C_{carb}$ and $\delta^{13}C_{org}$ data were

reported at the T-J boundary, indicating a global-scale carbon cycle disturbance. These excursions were preceded by a pronounced negative δ¹⁵N_{bulk} excursion caused by direct assimilation of ¹⁵Ndepleted NH₄₊ by marine eukaryotes likely via water column upwelling. The elevated P content indicates the elevated primary productivity, which would have triggered organic matter export and thereby simulating bottom-water oxygen depletion and the development of euxinia as evidenced by pyrite size distributions and a long-term decline in biotic abundance predate the T-J boundary. The eutrophication from upwelling and shallow marine euxinia likely triggered severe ecological stress on the carbonate platform and killed most of the carbonate-producing skeletal fauna, which were the main contributors to carbonate factory. Enhanced terrigenous clastic input, as evidenced by increased Al and Ti concentrations, further influenced carbonate accumulation by turbidity and rapid sedimentary rates. The largescale volcanism linked to the CAMP, as indicated by Hg enrichment and negative CIEs, is most plausibly triggered rapid environmental changes and induced the ultimate carbonate platform demise.

Data availability statement

The raw data supporting the conclusions of this article will be made available by the authors, without undue reservation.

Ethics statement

Written informed consent was obtained from the individual(s) for the publication of any potentially identifiable images or data included in this article.

Author contributions

YZ: Writing – original draft, Writing – review & editing. HW: Writing – review & editing. AM: Writing – review & editing. YW: Writing – original draft. XF: Writing – review & editing.

Funding

The author(s) declare financial support was received for the research and/or publication of this article. This work was supported by the National Natural Science Foundation of China (grant numbers: 42241202, 42272118, 42241203, and W2433105).

Acknowledgments

We thank associated editor and two reviewers for their constructive comments.

References

Al-Suwaidi, A. H., Steuber, T., and Suarez, M. B. (2016). The Triassic-Jurassic boundary event from an equatorial carbonate platform (Ghalilah Formation, United Arab Emirates). *J. Geological Soc.* 173, 949–953. doi: 10.1144/jgs2015-102

Amanda, M. O., and Peter, K. S. (2014). Interpreting carbonate and organic carbon isotope covariance in the sedimentary record. *Nat. Commun.* 5, Article 4672. doi: 10.1038/ncomms5672

Angiolini, L., Balini, M., Garzanti, E., Nicora, A., and Tintori, A. (2003). Gondwanan deglaciation and opening of Neotethys: The Al Khlata and Saiwan formations of Interior Oman. *Palaeogeogr. Palaeoclimatol. Palaeoecol.* 196, 99–123. doi: 10.1016/S0031-0182(03)00315-8

Bachan, A., and Payne, J. L. (2016). Modelling the impact of pulsed CAMP volcanism on pCO2 and δ 13C across the Triassic-Jurassic transition. *Geological Magazine* 153(2), 252–270.

Bahamonde, J. R., Colmenero, J. R., and Vera, C. (1997). Growth and demise of Late Carboniferous carbonate platforms in the eastern Cantabrian Zone, Asturias, northwestern Spain. *Sedimentary Geology* 110 (1–2), 99–122.

Beerling, D. J., and Berner, R. A. (2002). Biogeochemical constraints on the Triassic-Jurassic boundary carbon cycle event. *Global Biogeochemical Cycles* 16 (3), 1036.

Berner, R. (2003). The long-term carbon cycle, fossil fuels and atmospheric composition. *Nature* 426, 323–326.

Betzler, C., Hübscher, C., Lindhorst, S., Lüdmann, T., Hincke, C., Beaman, R. J., et al (2024). Seismic stratigraphic and sedimentary record of a partial carbonate platform drowning, Queensland Plateau, north-east Australia. *Marine Geology* 470, 107255.

Brçiź, V., Glumac, B., Brlek, M., Fuçek, L., and Miko, M. Š. (2021). Cenomanian-Turonian oceanic anoxic event (OAE2) imprint on the northwestern part of the Adriatic Carbonate Platform and a coeval intra-platform basin (Istria and Premuda Island, Croatia). *Cretaceous Research* 125, 104847.

Carter, E. S., and Hori, R. S. (2005). Global correlation of the radiolarian faunal change across the Triassic-Jurassic boundary. *Can. J. Earth Sci.* 42, 777–790. doi: 10.1139/e05-020

Chen, M., Fu, X., Wang, J., Wei, H., Zhang, Q., and Mansour, A. (2023). Tethyan ocean acidification triggered the end-Triassic mass extinction: New Ca isotopic

Conflict of interest

The authors declare that the research was conducted in the absence of any commercial or financial relationships that could be construed as a potential conflict of interest.

Generative AI statement

The author(s) declare that no Generative AI was used in the creation of this manuscript.

Any alternative text (alt text) provided alongside figures in this article has been generated by Frontiers with the support of artificial intelligence and reasonable efforts have been made to ensure accuracy, including review by the authors wherever possible. If you identify any issues, please contact us.

Publisher's note

All claims expressed in this article are solely those of the authors and do not necessarily represent those of their affiliated organizations, or those of the publisher, the editors and the reviewers. Any product that may be evaluated in this article, or claim that may be made by its manufacturer, is not guaranteed or endorsed by the publisher.

constraints from the Qiangtang Basin. Gondwana Res. 124, 206-217. doi: 10.1016/j.gr.2023.07.009

Chen, W. X., and Wang, J. (2009). Correlation of Upper Triassic strata in Qiangtang Basin, northern Tibet, Geology in China 36 (04), 809–818. doi: 10.3969/j.issn.1000-3657.2009.04.007

Davies, J., Marzoli, A., Bertrand, H., Youbi, N., Ernesto, M., and Schaltegger, U. (2017). End-Triassic mass extinction started by intrusive CAMP activity. *Nat. Commun.* 8, 15596. doi: 10.1038/ncomms15596

Derry, L. A., Brasier, M. D., Corfield, R. M., Rozanov, A. Yu, and Zhuravlev, A. (1994). Sr and C isotopes in Lower Cambrian carbonates from the Siberian craton: A paleoenvironmental record during the Cambrian explosion. *Earth Planetary Sci Lett.* 128, 671–681. doi: 10.1016/0012-821X(94)90178-3

Dickens, G. R., O'Neil, J. R., Rea, D. K., and Owen, R. M. (1995). Dissociation of oceanic methane hydrate as a cause of the carbon isotope excursion at the end of the Paleocene. *Paleoceanography* 10, 965–971. doi: 10.1029/95PA02087

Du, T., Wang, S., Jing, Z., Liu, X., Li, X., Wang, F., et al. (2024). Future changes in coastal upwelling and biological production in eastern boundary upwelling systems. *Nature Communications* 15, Article 6238.

Falkowski, P. (1997). Evolution of the nitrogen cycle and its influence on the biological sequestration of CO2 in the ocean. *Nature* 387, 272–275. doi: 10.1038/387272a0

Fang, X., Song, C., Yan, M., Zan, J., Liu, C., Sha, J., et al. (2016). Mesozoic litho- and magneto-stratigraphic evidence from the central Tibetan Plateau for megamonsoon evolution and potential evaporites. *Gondwana Res.* 37, 110–129. doi: 10.1016/j.gr.2016.05.012

Felber, R., Weissert, H. J., Furrer, H., and Hautmann, M. (2015). The Triassic-Jurassic boundary in the shallow-water marine carbonates from the western Northern Calcareous Alps (Austria). *Swiss J. Geosciences* 108, 213–224. doi: 10.1007/s00015-015-0192-1

Flügel, E., and Kiessling, W. (2002). Patterns of Phanerozoic reef crises. Soc. Sedimentary Geol., 72. doi: 10.2110/pec.02.72.0691

Föllmi, K. B., and Gainon, F. (2008). Demise of the northern Tethyan Urgonian carbonate platform and subsequent transition towards pelagic conditions: The

sedimentary record of the Col de la Plaine Morte area, central Switzerland. Sedimentary Geol. 205, 142–159. doi: 10.1016/j.sedgeo.2008.02.005

- Font, E., Chen, J., Regelous, M., Regelous, A., and Adatte, T. (2021). Volcanic origin of the mercury anomalies at the Cretaceous-Paleogene transition of Bidart, France. *Geology* 50, 142–146. doi: 10.1130/G49458.1
- Fox, C. P., Whiteside, J. H., Olsen, P. E., Cui, X. Q., Summons, R. E., Idiz, E., et al. (2022). Two-pronged kill mechanism at the end-Triassic mass extinction. *Geology* 50, 448–453. doi: 10.1130/G49560.1
- Freudenthal, T., Wagner, T., Wenzhöfer, F., Matthias, F., and Gerold, W. (2001). Early diagenesis of organic matter from sediments of the eastern subtropical Atlantic: Evidence from stable nitrogen and carbon isotopes. *Geochimica Cosmochimica Acta* 65, 1795–1808. doi: 10.1016/S0016-7037(01)00554-3
- Fu, X., Wang, J., Tan, F., Chen, M., Li, Z., Zeng, Y., et al. (2016). New insights about petroleum geology and exploration of Qiangtang Basin, northern Tibet, China: A model for low-degree exploration. *Mar. Petroleum Geol.* 77, 323–340. doi: 10.1016/j.marpetgeo.2016.06.015
- Fujisaki, W., Fukami, Y., Matsui, Y., Sato, T., Sawaki, Y., and Suzuki, K. (2020). Redox conditions and nitrogen cycling during the Triassic-Jurassic transition: A new perspective from the mid-Panthalassa. *Earth-Science Rev.* 204, 103173. doi: 10.1016/j.earscirev.2020.103173
- Fyhn, M. B. W., Boldreel, L. O., Nielsen, L. H., Giangc, T. C., Ngac, L. H., Hongd, T. M., et al. (2013). Carbonate platform growth and demise offshore Central Vietnam: Effects of Early Miocene transgression and subsequent onshore uplift. *J. Asian Earth Sci.* 76, 152–168. doi: 10.1016/j.jseaes.2013.02.023
- Galli, M. T., Jadoul, F., Bernasconi, S. M., and Weissert, H. (2005). Anomalies in global carbon cycling and extinction at the Triassic/Jurassic boundary: Evidence from a marine C-isotope record. *Palaeogeogr. Palaeoclimatol. Palaeoecol.* 216, 203–214. doi: 10.1016/j.palaeo.2004.11.009
- Gaździcki, A., Kozur, H., and Mock, R. (1979). The Norian-Rhaetian boundary in the light of micropaleontological data. *Geologija* 22, 71–112.
- Ge, Y., Shi, M., Steuber, T., Al-Suwaidi, A. H., Suarez, M. B., et al. (2018). Environmental change during the Triassic-Jurassic boundary interval of an equatorial carbonate platform: Sedimentology and chemostratigraphy of the Ghalilah Formation, United Arab Emirates. *Palaeogeography, Palaeoclimatology, Palaeoecology* 502, 86–103.
- Grasby, S. E., Them, T. R., Chen, Z., Yin, R., and Ardakani, O. H. (2019). Mercury as a proxy for volcanic emissions in the geologic record. *Earth-Science Rev.* 196, 102880. doi: 10.1016/j.earscirev.2019.102880
- Greene, S. E., Martindale, R. C., Ritterbush, K. A., Bottjer, D. J., Corsetti, F. A., and Berelson, W. M. (2012). Recognising ocean acidification in deep time: An evaluation of the evidence for acidification across the Triassic-Jurassic boundary. *Earth-Science Rev.* 113, 72–93. doi: 10.1016/j.earscirev.2012.03.009
- Guevara, S. R., Meili, M., Rizzo, A., Daga, R., and Arribère, M. (2010). Sediment records of highly variable mercury inputs to mountain lakes in Patagonia during the past millennium. *Atmospheric Chem. Phys.* 10, 3443–3453. doi: 10.5194/acp-10-3443-2010
- Hallock, P., and Schlager, W. (1986). Nutrient Excess and the Demise of Coral Reefs and Carbonate Platforms. Palaios 1 (4), 389–398. doi: 10.2307/3514476
- Hautmann, M., Benton, M. J., and Tomašových, A. (2008). Catastrophic ocean acidification at the Triassic-Jurassic boundary. *Neues Jahrbuch für Geologie und Paläontologie Abhandlungen* 249, 119–127. doi: 10.1127/0077-7749/2008/0249-0119
- Heimdal, T. H., Jones, M. T., and Svensen, H. H. (2020). Thermogenic carbon release from the Central Atlantic magmatic province caused major end-Triassic carbon cycle perturbations. *Proceedings of the National Academy of Sciences* 117 (22), 11968–11974.
- Hesselbo, S. P., Gröcke, D. R., Jenkyns, H. C., Bjerrum, C. J., Farrimond, P., Morgans Bell, H. S., et al. (2000). Massive dissociation of gas hydrate during a Jurassic oceanic anoxic event. *Nature* 406, 392–395. doi: 10.1038/35019044
- Hesselbo, S. P., Robinson, S. A., Surlyk, F., and Piasecki, S. (2002). Terrestrial and marine extinction at the Triassic-Jurassic boundary synchronized with major carboncycle perturbation: A link to initiation of massive volcanism? *Geology* 30, 251–254. doi: 10.1130/0091-7613(2002)030<0251:TAMEAT>2.0.CO;2
- Higgins, M. B., Robinson, R. S., Husson, J. M., Carter, S. J., and Pearson, A. (2012). Dominant eukaryotic export production during ocean anoxic events reflects the importance of recycled NH₄⁺. *Proc. Natl. Acad. Sci.* 109, 2269–2274. doi: 10.1073/pnas.1104313109
- Hou, M., Deng, M., Shi, H., Liu, J., Wang, R., Zeng, Y., et al. (2017). The process of growth, development and extinction of the Early Miocene carbonate rocks and controlling factors in the Pearl River Mouth Basin. *Acta Petrologica Sin*. Beijing 33, 1257–1271.
- Jiang, W., Yu, K., Fan, T., Xu, D., Wang, R., Zhang, Y., et al. (2019). Coral reef carbonate record of the Pliocene-Pleistocene climate transition from an atoll in the South China Sea. *Mar. Geol.* 411, 88–97. doi: 10.1016/j.margeo.2019.02.006
- Junium, C. K., and Arthur, M. A. (2007). Nitrogen cycling during the Cretaceous, Cenomanian-Turonian Oceanic Anoxic Event II. *Geochem. Geophys. Geosystems* 8, Q03002. doi: 10.1029/2006GC001328
- Kametaka, M., Takebe, M., Nagai, H., Zhu, S., and Takayanagi, Y. (2005). Sedimentary environments of the Middle Permian phosphorite-chert complex from

the northeastern Yangtze platform, China; the Gufeng Formation: a continental shelf radiolarian chert. Sedimentary Geol. 174, 197–222. doi: 10.1016/j.sedgeo.2004.12.005

- Kasprak, A. H., Sepúlveda, J., Price-Waldman, R., Williford, K. H., Schoepfer, S. D., Haggart, J. W., et al. (2015). Episodic photic zone euxinia in the northeastern Panthalassic Ocean during the end-Triassic extinction. *Geology* 43, 307–310. doi: 10.1130/G36371.1
- Kaufman, A. J., Knoll, A. H., and Narbonne, G. M. (1997). Isotopes, ice ages, and terminal Proterozoic earth history. *Proc. Natl. Acad. Sci.* 94, 6600–6605. doi: 10.1073/pnas.94.13.6600
- Kiessling, W., Aberhan, M., Brenneis, B., and Wagner, P. J. (2007). Extinction trajectories of benthic organisms across the Triassic-Jurassic boundary. *Palaeogeogr. Palaeoclimatol. Palaeoecol.* 244, 201–222. doi: 10.1016/j.palaeo.2006.06.029
- Knoll, A. H., Hayes, J. M., Kaufman, A. J., and Swett, K. (1986). Secular variation in carbon isotope ratios from Upper Proterozoic successions of Svalbard and East Greenland. *Nature* 321, 832–838. doi: 10.1038/321832a0
- Korte, C., Jasper, T., Kozur, H. W., and Veizer, J. (2006). $\rm ^{87}Sr/^{86}Sr$ record of Permian seawater. *Palaeogeogr. Palaeoclimatol. Palaeoecol.* 240, 89–107. doi: 10.1016/j.palaeo.2006.03.047
- Krishnamurthy, R. V., and Bhattacharya, S. K. (1986). Palaeoclimatic changes deduced from $^{13}\text{C}/^{12}\text{C}$ and C/N ratios of Karewa lake sediments, India. *Nature* 323, 150–152. doi: 10.1038/323150a0
- Kuypers, M. M. M., van Breugel, Y., Schouten, S., Erba, E., and Sinninghe Damsté, J. S. (2004). N_2 -fixing cyanobacteria supplied nutrient N for Cretaceous oceanic anoxic events. *Geology* 32, 853–856. doi: 10.1130/G20458.1
- Lehmann, M. F., Bernasconi, S. M., Barbieri, A., and McKenzie, J. A. (2002). Preservation of organic matter and alteration of its carbon and nitrogen isotope composition during simulated and in *situ* early sedimentary diagenesis. *Geochimica Cosmochimica Acta* 66, 3573–3584. doi: 10.1016/S0016-7037(02)00968-7
- Leonide, P., Floquet, M., Durlet, C., Baudin, F., Pittet, B., and Lécuyer, C. (2012). Drowning of a carbonate platform as a precursor stage of the Early Toarcian global anoxic event (Southern Provence sub-Basin, South-east France). *Sedimentology* 59, 156–184. doi: 10.1111/j.1365-3091.2010.01221.x
- Li, J., Gao, P., Xiao, X., Lash, G. G., Li, S., Liu, W., et al (2024). Widespread coastal upwelling along the marginal Yangtze Platform (South China) during the early Cambrian: Implications for hyper-enrichment of organic matter. *Palaeogeography, Palaeoclimatology, Palaeoecology* 656, 112569.
- Li, J., Song, H., Du, Y., Wignall, P. B., Bond, D. P. G., Grasby, S. E., et al (2025). Spatial and temporal heterogeneity of the marine nitrogen cycle during the end-Triassic mass extinction. *Chemical Geology* 682, 122752.
- Lindström, S., Callegaro, S., Davies, J., Tegner, C., van de Schootbrugge, B., Pedersen, G. K., et al. (2021). Tracing volcanic emissions from the Central Atlantic Magmatic Province in the sedimentary record. *Earth-Science Rev.* 212, 103444. doi: 10.1016/jearscirev.2020.103444
- Liu, J., Qie, W., Algeo, T. J., Yao, L., Huang, J. H., and Luo, G. (2016). Changes in marine nitrogen fixation and denitrification rates during the end-Devonian mass extinction. *Palaeogeogr. Palaeoclimatol. Palaeoecol.* 448, 195–206. doi: 10.1016/j.palaeo.2015.10.022
- Liu, J., Zhou, W., Li, Y., Qiu, D., Liu, D., Lin, J., et al. (2007). Analysis and evaluation of oil and gas resource potential in the Qinghai-Tibet region (Beijing: Geological Publishing House).
- Luan, G., Lin, C., Azmy, K., Fu, L., Dong, C. H., Liu, H., et al. (2024). Marine anoxia events across the upper Cambrian (stage 10) of eastern Gondwana: Implications from paleoenvironmental geochemical proxies. *Mar. Petroleum Geol.* 164, 106789. doi: 10.1016/j.marpetgeo.2024.106813
- Marino, M., and Santantonio, M. (2010). Understanding the geological record of carbonate platform drowning across rifted Tethyan margins: Examples from the Lower Jurassic of the Apennines and Sicily (Italy). *Sedimentary Geol.* 225, 116–137. doi: 10.1016/j.sedgeo.2010.02.002
- Martínez-Rodríguez, R., Castro, J. M., de Gea, G. A., Nieto, L. M., Ruiz-Ortiz, P. A., Skelton, P. W., et al (2025). Early Aptian development and OAE 1a-linked demise of a carbonate platform in the western Tethys: Lower Cretaceous of Sierra Mariola (South Iberian Paleomargin, SE Spain). *Cretaceous Research* 167, 106032.
- Maurer, F., Rettori, R., and Martini, R. (2008). Triassic stratigraphy, facies and evolution of the Arabian shelf in the northern United Arab Emirates. *Int. J. Earth Sci.* 97, 765–784. doi: 10.1007/s00531-007-0194-y
- Mazrui, N. M., Jonsson, S., Thota, S., Zhao, J., and Mason, R. P. (2016). Enhanced availability of mercury bound to dissolved organic matter for methylation in marine sediments. *Geochimica Cosmochimica Acta* 194, 153–162. doi: 10.1016/j.gca.2016.08.019
- McElwain, J. C., Beerling, D. J., and Woodward, F. I. (1999). Fossil plants and global warming at the Triassic-Jurassic boundary. *Science* 285, 1386–1390. doi: 10.1126/science.285.5432.1386
- McRoberts, C. A., Furrer, H., and Jones, D. S. (1997). Palaeoenvironmental interpretation of a Triassic-Jurassic boundary section from Western Austria based on palaeoecological and geochemical data. *Palaeogeogr. Palaeoclimatol. Palaeoecol.* 136, 79–95. doi: 10.1016/S0031-0182(97)00074-6

McRoberts, C. A., Krystyn, L., and Hautmann, M. (2012). Macrofaunal response to the end-Triassic mass extinction in the west-Tethyan Kössen Basin, Austria. *PALAIOS* 27, 607–616. doi: 10.2110/palo.2012.p12-043r

Metcalfe, I. (2013). Gondwana dispersion and Asian accretion: Tectonic and palaeogeographic evolution of Eastern Tethys. *J. Asian Earth Sci.* 66, 1–33. doi: 10.1016/j.jseaes.2012.12.020

Montanaro, A., Falzoni, F., Iannace, A., and Parente, M. (2024). Patterns of extinction and recovery across the Triassic-Jurassic boundary interval in three resilient Southern Tethyan carbonate platforms. *Palaeogeogr. Palaeoclimatol. Palaeoccol.* 649, 112335. doi: 10.1016/j.palaeo.2024.112335

Mutti, M., and Hallock, P. (2003). Carbonate systems along nutrient and temperature gradients: some sedimentological and geochemical constraints. *Int. J. Earth Sci.* 92, 465–475. doi: 10.1007/s00531-003-0350-y

Oehlert, A. M., and Swart, P. K. (2014). Interpreting carbonate and organic carbon isotope covariance in the sedimentary record. *Nature Communications* 5, 4672.

Pálfy, J. (2003). Volcanism of the Central Atlantic Magmatic Province as a potential driving force in the end-Triassic mass extinction. *Geophysical Monograph Ser.* 136, 255–267. doi: 10.1029/136GM014

Pálfy, J., Demény, A., Hetényi, M., Haas, J., Orchard, M. J., and Veto, I. (2001). Carbon isotope anomaly and other geochemical changes at the Triassic-Jurassic boundary. *Geology* 29, 1047–1050. doi: 10.1130/0091-7613(2001)029<1047: CIAAOG-2.0.CO:2

Pálfy, J., Kovács, Z., Demény, A., and Vallner, Z. (2021). End-Triassic crisis and "unreefing" led to the demise of the Dachstein carbonate platform: A revised model and evidence from the Transdanubian Range, Hungary. *Global Planetary Change* 199, 103428. doi: 10.1016/j.gloplacha.2021.103428

Pantoja, S., Repeta, D. J., Sachs, J. P., and Sigman, D. M. (2002). Stable isotope constraints on the nitrogen cycle of the Mediterranean Sea water column. *Deep Sea Res. Part I* 49, 1609–1621. doi: 10.1016/S0967-0637(02)00066-3

Park, R., and Epstein, S. (1960). Carbon isotope fractionation during photosynthesis. *Geochimica Cosmochimica Acta* 21, 110–126. doi: 10.1016/S0016-7037(60)80006-3

Paul, A., López-Otálvaro, G.-E., and Reijmer, J. J. G. (2025). Sedimentation dynamics on the Maldives carbonate platform in response to Quaternary monsoonal forcing and sea-level changes. *Mar. Geol.* 485, 107561. doi: 10.1016/j.margeo.2025.107561

Philip, J. M., and Airaud-Crumière, C. (1991). The demise of the rudist-bearing carbonate platforms at the Cenomanian/Turonian boundary: A global control. *Coral Reefs* 10, 115–125. doi: 10.1007/BF00571829

Pyle, D. M., and Mather, T. A. (2003). The importance of volcanic emissions for the global atmospheric mercury cycle. *Atmospheric Environ*. 37, 5115–5124. doi: 10.1016/j.atmosenv.2003.07.011

Quan, T., van de Schootbrugge, B., Field, M. P., Rosenthal, Y., and Falkowski, P. G. (2008). Nitrogen isotope and trace metal analyses from the Mingolsheim core (Germany): Evidence for redox variations across the Triassic-Jurassic boundary. *Global Biogeochemical Cycles* 22, GB2013. doi: 10.1029/2007GB002981

Raiswell, R. (1982). Pyrite texture, isotopic composition and the availability of iron. Am. J. Sci 282, 1244–1263. doi: 10.2475/ajs.282.8.1244

Ravichandran, M. (2004). Interactions between mercury and dissolved organic matter—a review. *Chemosphere* 55, 319–331. doi: 10.1016/j.chemosphere.2003.11.011

Rigo, M., Favero, M., Di Stefano, P., and Todaro, S. (2024). Organic carbon isotope (\$^{19}C_{org}) curve and extinction trends across the Triassic/Jurassic boundary at Mt. Sparagio (Italy): A tool for global correlations between peritidal and pelagic successions. *Palaeogeogr. Palaeoclimatol. Palaeoecol.* 654, 112440. doi: 10.1016/j.palaeo.2024.112440

Ruhl, M., Hesselbo, S. P., Al-Suwaidi, A., Jenkyns, H. C., Damborenea, S. E., Manceñido, M. O., et al. (2020). On the onset of Central Atlantic Magmatic Province (CAMP) volcanism and environmental and carbon-cycle change at the Triassic-Jurassic transition (Neuquén Basin, Argentina). *Earth-Science Rev.* 208, 103270. doi: 10.1016/j.earscirev.2020.103229

Ruhl, M., and Kürschner, W. M. (2011). Multiple phases of carbon cycle disturbance from large igneous province formation at the Triassic-Jurassic transition. *Geology* 39, 431–434. 127. doi: 10.1130/G31680.1

Ruhl, M., Veldb, H., and Kürschner, W. M. (2010). Sedimentary organic matter characterization of the Triassic–Jurassic boundary GSSP at Kuhjoch (Austria). *Earth Planetary Sci Lett.* 292, 17–26. doi: 10.1016/j.epsl.2009.12.046

Ruvalcaba Baroni, I., van Helmond, N., Tsandev, I., Middelburg, J., and Slomp, C. (2015). The nitrogen isotope composition of sediments from the proto-North Atlantic during Oceanic Anoxic Event 2. *Paleoceanography* 30, 923–937. doi: 10.1002/2014PA002744

Sachs, J. P., and Repeta, D. J. (1999). Oligotrophy and nitrogen fixation during eastern Mediterranean sapropel events. *Science* 286 (5449), 2485–2488.

Saltzman, M. R., and Thomas, E. (2012). Chapter 11 - Carbon Isotope Stratigraphy. In F. M. Gradstein, G. J. Ogg, M. D. Schmitz and G. M. Ogg (Eds.). *The Geologic Time Scale* (Elsevier), 207–232.

Sawlowicz, Z. (1993). Pyrite framboids and their development: A new conceptual mechanism. *Geologische Rundschau* 82, 148–156. doi: 10.1007/BF00563277

Schlager, W. (1981). The paradox of drowned reefs and carbonate platforms. GSA Bull. 92, 197–211. doi: 10.1130/0016-7606(1981)92<197:TPODRA>2.0.CO;2

Schoepfer, S. D., Algeo, T. J., Ward, P. D., Williford, K. H., and Haggart, J. W. (2016). Testing the limits in a greenhouse ocean: Did low nitrogen availability limit marine productivity during the end-Triassic mass extinction? *Earth Planetary Sci Lett.* 451, 138–148. doi: 10.1016/j.epsl.2016.06.050

Schuster, P. F., Krabbenhoft, D. P., Naftz, D. L., Cecil, L. D., Olson, M. L., Dewild, J. F., et al. (2002). Atmospheric mercury deposition during the last 270 years: A glacial ice core record of natural and anthropogenic sources. *Environ. Sci Technol.* 36, 2303–2310. doi: 10.1021/es0157503

Selin, N. E. (2009). Global biogeochemical cycling of mercury: A review. *Annu. Rev. Environ. Resour.* 34, 43–63. doi: 10.1146/annurev.environ.051308.084314

Sengör, A. M. C. (1979). Mid-Mesozoic closure of Permo-Triassic Tethys and its implications. *Nature* 279, 590–593. doi: 10.1038/279590a0

Shen, J., Yin, R., Zhang, S., Algeo, T. J., Bottjer, D. J., Yu, J., et al (2022). Intensified continental chemical weathering and carbon-cycle perturbations linked to volcanism during the Triassic-Jurassic transition. *Nature Communications* 13, Article 299.

Sigman, D. M., Karsh, K. L., and Casciotti, K. L. (2009). "Nitrogen isotopes in the ocean," in *Encyclopedia of ocean sciences*, America *2nd ed.* Ed. J. H. Steele, et al (America: Elsevier), 40–54.

Song, P., Ding, L., Li, Z., Lippert, P., and Yue, Y. (2017). An early bird from Gondwana: Paleomagnetism of Lower Permian lavas from Northern Qiangtang (Tibet) and the geography of the Paleo-Tethys. *Earth Planetary Sci Lett.* 475, 119–133. doi: 10.1016/j.epsl.2017.07.023

Song, C., Wang, J., Fu, X., Feng, X., Chen, M., and He, L. (2012). Late Triassic paleomagnetic data from the Qiangtang Terrane of Tibetan Plateau and their tectonic significance. *J. Jilin Univ.* (Earth Sci Edition) 42, 526–535. doi: 10.16539/j.ddgzyckx.2012.01.001

Stampfli, G. M., and Borel, G. D. (2002). A plate tectonic model for the Paleozoic and Mesozoic constrained by dynamic plate boundaries and restored synthetic oceanic isochrons. *Earth Planetary Sci Lett.* 196, 17–33. doi: 10.1016/S0012-821X(01) 00588-X

Stüeken, E. E., Gregory, D. D., Mukherjee, I., and McGoldrick, P. (2021). Sedimentary exhalative venting of bioavailable nitrogen into the early ocean. *Earth Planetary Sci Lett.* 565, 116914. doi: 10.1016/j.epsl.2021.116963

Stücken, E. E., Kipp, M. A., Koehler, M. C., and Buick, R. (2016). The evolution of Earth's biogeochemical nitrogen cycle. *Earth-Science Rev.* 160, 220–239. doi: 10.1016/j.earscirev.2016.07.007

Tan, F., Wang, J., Wang, X., and Du, B. (2002). The Qiangtang Basin in Xizang as the target area for the oil and gas resources in China. *Sedimentary Geol. Tethyan Geol.* 22, 16–21.

Todaro, S., Di Stefano, P., Zarcone, G., and Randazzo, V. (2017). Facies stacking and extinctions across the Triassic–Jurassic boundary in a peritidal succession from western Sicily. *Facies* 63, 20. doi: 10.1007/s10347-017-0500-5

Todaro, S., Rigo, M., Di Stefano, P., Aiuppa, A., and Chiaradia, M. (2022). Endtriassic extinction in a carbonate platform from western tethys: A comparison between extinction trends and geochemical variations. *Front. Earth Sci* 10, Article 850898. doi: 10.3389/feart.2022.875466

Trecalli, A., Spangenberg, J., Adatte, T., Föllmi, K. B., and Parente, M. (2012). Carbonate platform evidence of ocean acidification at the onset of the early Toarcian oceanic anoxic event. *Earth Planetary Sci Lett.* 357-358, 214–225. doi: 10.1016/j.epsl.2012.09.043

Tyrrell, T. (1999). The relative influences of nitrogen and phosphorus on oceanic primary production. Nature~400, 525-531.~doi: 10.1038/22941

Tyson, R. V., and Pearson, T. H. (1991). Modern and ancient continental shelf anoxia: an overview. *Geological Society London Special Publications* 58, 1–24. doi: 10.1144/GSL.SP.1991.058.01.01

Urban, I., Demangel, I., Krystyn, L., Calner, M., Kovács, Z., Gradwohl, G., et al. (2023). Mid-Norian to Hettangian record and time-specific oolites during the end-Triassic Mass Extinction at Wadi Milaha, Musandam Peninsula, United Arab Emirates. *J. Asian Earth Sciences: X* 9, 100138. doi: 10.1016/j.jaesx.2023.100138

van de Schootbrugge, B., Payne, J. L., Tomasovych, A., Pross, J., Fiebig, J., Benbrahim, M., et al. (2008). Carbon cycle perturbation and stabilization in the wake of the Triassic-Jurassic boundary mass-extinction event. *Geochem. Geophys. Geosystems* 9, Article Q04S04. doi: 10.1029/2007GC001914

Veizer, J., Ala, D., Azmy, K., and Bruckschen, P. (1999). $^{87}Sr/^{86}Sr,\,\delta^{13}C$ and $\delta^{18}O$ evolution of Phanerozoic seawater. Chem. Geol. 161, 59–88. doi: 10.1016/S0009-2541 (99)00081-9

Wang, J., Ding, J., Wang, C. S., and Tan, F. W. (2009). Potential analysis and geological survey of the hydrocarbon resources in Tibetan Plateau (Beijing: Geological Publishing House, Beijing).

Wang, J., and Fu, X. G. (2018). Sedimentary evolution of the qiangtang basin. *Geol. China* 45, 237–258. doi: 10.16509/j.georeview.2020.05.002

Wang, J., Fu, X. G., Shen, L. J., Tan, F. W., Song, C. Y., and Chen, W. B. (2020). Prospect of the potential of oil and gas resources in Qiangtang Basin, Xizang (Tibet). *Geological Rev.* 66, 1091–1113.

Wang, J., Fu, X., Wei, H., Shen, L., Wang, Z., and Li, K. (2022). Late Triassic basin inversion of the Qiangtang Basin in northern Tibet: Implications for the closure of the

Paleo-Tethys and expansion of the Neo-Tethys. J. Asian Earth Sci. 227, 105119. doi: 10.1016/j.jseaes.2022.105119

Wang, J., Tan, F., Li, Y., Li, Y., Chen, M., Wang, C., et al. (2004). The potential of the oil and gas resources in major sedimentary basins on the Qinghai-Xizang Plateau (Beijing: Geological Publishing House, Beijing).

Wang, Y., and Zheng, C. (2007). Lithostratigraphy, sequence stratigraphy and biostratigraphy of the Sobucha and Quse formations and the Triassic-Jurassic boundary in the Sewa area on the south margin of the Qiangtang Basin, Northern Tibet. *J. Stratigraphy* 31, 379–387.

Ward, P. D., Haggart, J. W., Carter, E. S., Wilbur, D., Tipper, H. W., and Evans, T. (2001). Sudden productivity collapse associated with the Triassic-Jurassic boundary mass extinction. *Science* 292, 1148–1151. doi: 10.1126/science.1058574

Wilkin, R. T., Barnes, H. L., and Brantley, S. L. (1996). The size distribution of framboidal pyrite in modern sediments: An indicator of redox conditions. *Geochimica Cosmochimica Acta* 60, 3897–3912. doi: 10.1016/0016-7037(96)00209-8

Wilson, M. E. J. (2008). Global and regional influences on equatorial shallow-marine carbonates during the Cenozoic. *Palaeogeogr. Palaeoclimatol. Palaeoecol.* 26, 262–274. doi: 10.1016/j.palaeo.2008.05.012

Wu, S., Qin, Y., Ma, Y., and Tian, L. (2022). Proposal for scientific drilling of carbonate platforms in the South China Sea: Revealing the controlling factors and drowning mechanisms of carbonate platforms. *Acta Geologica Sin.* 96, 2809–2821. doi: 10.19762/j.cnki.dizhixuebao.2022066

Yan, Y., Huang, B., Zhang, D., Charusiri, P., and Veeravinantanakul, A. (2018). Paleomagnetic study on the Permian rocks of the IndoChina Block and its implications

for paleogeographic configuration and northward drifting of Cathaysialand in the Paleo-Tethys. *J. Geophysical Research: Solid Earth* 123, 4523–4538. doi: 10.1029/2018JB015511

Zaffani, M., Jadoul, F., and Rigo, M. (2018). A new Rhaetian $\delta^{13}C_{org}$ record: Carbon cycle disturbances, volcanism, End-Triassic mass Extinction (ETE). *Earth-Science Rev.* 178, 92–104. doi: 10.1016/j.earscirev.2018.01.004

Zeng, S., Wang, J., Chen, W., Fu, X., Yan, Z., Li, J., et al. (2019). Zircon U-Pb age of volcaniclastic rock from the upper part of E'er Longba Formation in eastern Qiangtang Basin of Tibet. *Geol. China* 46, 1573–1575. doi: 10.12029/gc20190621

Zhang, X., Gao, Y., Chen, X., Hu, D., Li, M., Wang, C. H., et al. (2019). Nitrogen isotopic composition of sediments from the eastern Tethys during Oceanic Anoxic Event 2. *Palaeogeogr. Palaeoclimatol. Palaeoecol.* 515, 123–133. doi: 10.1016/j.palaeo.2018.03.013

Zhang, X., Hu, X., Li, J., and Xu, Y. (2024). Sedimentology and carbon isotope records of latest early Permian carbonate platform drowning event in lower yangtze region. *Geological J. China Universities* 30, 379–396. doi: 10.16108/j.issn1006-7493.2023030

Zhang, X., Ward, B. B., and Sigman, D. M. (2020). Global nitrogen cycle: Critical enzymes, organisms, and processes for nitrogen budgets and dynamics. *Chem. Rev.* 120, 5308–5351. doi: 10.1021/acs.chemrev.9b00613

Zhao, Z., Li, Y., Ye, H., and Zhang, Y. (2001). Tectonic characteristics and basin evolution of the Tibetan Plateau (Beijing: Science Press, Beijing).

Zhu, R., Zhao, P., and Zhao, L. (2022). Tectonic evolution and geodynamics of the Neo-Tethys Ocean. *Sci China Earth Sci.* 65, 1–24. doi: 10.1007/s11430-021-9845-7